ACTIVE CONTROL OF A THIN DEFORMABLE IN-PLANE ACTUATED MIRROR

THESIS

Thomas Paul Gabriele Jr, Captain, USAF

AFIT/GA/ENY/07-M07

DEPARTMENT OF THE AIR FORCE
AIR UNIVERSITY

AIR FORCE INSTITUTE OF TECHNOLOGY

Wright-Patterson Air Force Base, Ohio

The views expressed in this thesis are those of the author and do not reflect the official policy or position of the United States Air Force, Department of Defense, or the U.S. Government.

AFIT/GA/ENY/07-M07

ACTIVE CONTROL OF A THIN DEFORMABLE IN-PLANE ACTUATED MIRROR

THESIS

Presented to the Faculty

Department of Aeronautics and Astronautics

Graduate School of Engineering and Management

Air Force Institute of Technology

Air University

Air Education and Training Command

In Partial Fulfillment of the Requirements for the

Degree of Master of Science in Astronautical Engineering

Thomas Paul Gabriele Jr., BSE

Captain, USAF

March 2007

AFIT/GA/ENY/07-M07

ACTIVE CONTROL OF A THIN DEFORMABLE IN-PLANE ACTUATED MIRROR

Thomas Paul Gabriele Jr., BSE

Captain, USAF

Approved:

/signed/	15 Mar 2007
Dr. Richard G. Cobb Chairman	Date
/signed/	16 Mar 2007
Dr. Anthony N. Palazotto, P.E. Member	Date
/signed/	16 Mar 2007
Dr. William P. Baker Member	Date

AFIT/GA/ENY/07-M07

Abstract

Previous work done in the area of active control for surface stabilization and shaping of a deformable membrane mirror at the Air Force Institute of Technology has demonstrated that active control with a simple gain correction is possible using a quasi-static closed-loop feedback on an in-plane actuated deformable membrane mirror. This research builds on that work beginning with the implementation of a new data acquisition system to increase the throughput of the current system. Next, recommended fabrication technique changes are implemented to create a new five-inch membrane-like optical mirror. Lastly, using this new equipment setup, this research begins the process of developing a non-linear controller to actively damp out higher frequency disturbances. The overall goal of providing greater system bandwidth and control of multiple Zernike polynomials has been initially demonstrated.

Table of Contents

Page

Page

List of Figures

Figure Page

List of Tables

ACTIVE CONTROL OF A THIN DEFORMABLE

IN-PLANE ACTUATED MIRROR

I. Background

1.1 Introduction

The space-based imaging and communication needs of the United States Air Force continue to grow exponentially in a technologically evolving world. Current optical capabilities are limited in resolution due to aperture size and weight. The resolution of two ground points observed from an orbital platform (Δx) is defined by (Equation 1.1) below, where R is the range from the satellite to ground and ($\Delta\theta$) is the Rayleigh Criterion. However, the Rayleigh Criterion (Equation 1.2) is defined as the wavelength (λ) divided by the aperture diameter (D). Equation 1.3 combines Equations 1.1 and 1.2 and illustrates that the larger the aperture size is the smaller the distance between the two points will be [10].

$$\Delta x = R\Delta\theta \tag{1.1}$$

$$\Delta\theta = \frac{\lambda}{D} \tag{1.2}$$

$$\Delta x = \frac{R\lambda}{D} \tag{1.3}$$

The largest launch platform currently employed by the United States is the Space Shuttle, which can place a payload that is 4.5 meter diameter weighing 56,000 lbs into orbit. One of the largest optical payloads currently on orbit is the Hubble Space Telescope with a 4.2 meter diameter [15]. Fabricated with ultra-low expansion glass with an areal density of 180 kg/m^2, it has a primary mirror a weight of approximately 23,000

lbs. Current NASA plans for the James Webb Space Telescope (JWST) scheduled for launched in 2011, is being designed with a primary aperture of 6.5 meters consisting of 18 hexagonal beryllium segments. With an areal density of 13.2 kg/m^2 this new material will provide a considerable weight savings with the final primary mirror assembly projected to weigh approximately 7,350 lbs [16]. The JWST represents a significant reduction in areal density, however further reductions are still desired.

An equally important issue concerning space based optical platforms is the attenuation of external and internal disturbances. These disturbances have a significant impact on pointing and imaging. Combining both weight savings and actuation for disturbance rejection, the research described herein focuses on an in-plane actuated deformable mirror to achieve these objectives. In-plane actuated deformable mirrors rely on actuation from either piezoelectric or other types of electro- or magnetostrictive actuators. These actuators create regions of strain offset from and parallel to the structure's neutral axis, thus imparting a surface curvature [30]. Alternative materials and fabrication techniques which may also lead to reductions in areal density currently being investigated and are briefly discussed in Chapter II.

1.2 Problem Statement

Experimentally demonstrating closed-loop dynamic feedback control of an in-plane actuated membrane mirror is the focus of the research. Previously completed work at the Air Force Institute of Technology (AFIT) has demonstrated open-loop deformations. Work has also been done to demonstrate closed-loop control, but met with limited success due to measurement/control system bandwidth limitations which caused the applied controller to be considered only quasi-statically (<< 1Hz), and only very low

frequency tracking was demonstrated. Closed-loop disturbance rejection was never demonstrated.

1.3 Scope

There are three objectives that this research must meet in order to be successful in demonstrating dynamic closed-loop control of an in-plane actuated deformable membrane mirror. The first objective is to setup and validate a new acquisition system using a National Instruments PXI Chassis combined with Labview®. This combination of hardware and software enables the user to tailor projects using a series of created VIs to capture Zernike Polynomials from a Wavescope® wavefront sensor built by Adaptive Optics Associates Inc. (AOA), and then generate the necessary voltages that are applied to correct for deformations on the mirror. Validation of the system will be accomplished by reproducing linear tests previously conducted on the same mirror as well as testing the frequency response of the system to determine a throughput rate. This will establish the achievable bandwidth that any new controller will be able to correct input disturbances. The second objective is to implement new fabrication techniques based on recommendations from previous work done at AFIT. These include redesigning the aluminum ring that the mirror is stretched across, evaporating the actuation patches onto the control surface and removing the reflective coating on the mirror surface. The third objective is to demonstrate dynamic closed-loop control of an in-plane actuated membrane mirror by characterizing a newly created mirror, developing a new controller software, and then demonstrating control of surface deflections as a small sinusoidal tilt disturbance is imposed on the mirror.

1.4 Summary

The research herein investigates fabrication and measurement/control system upgrades for an in-plane actuated deformable membrane mirror. Chapter II provides a summary overview of other current research into fabrication techniques, actuation methods and control algorithms, for large optics with a focus on topics relevant to this research. Chapter III describes changes to the data acquisition model and its validation. Chapter IV discusses test objectives, results, and assess if the objectives detailed in Section 1.3 were met. Finally Chapter V summarizes the work, draws conclusions, and recommendations for future research.

II. Literature Review

2.1 Overview

Traditional large glass mirrors are not a viable option for space applications because their rigidity limits the mirror diameter which can be placed on orbit. Capabilities of current generation launch vehicles are limited to approximately four meters. Moreover, according to the Center for Strategic and Budgetary Assessments, launch costs currently average around $10,000 per pound for a geostationary launch. These costs, coupled with the large areal density of glass, make traditional optics in space costly [38].

Table 2.1 CURRENT COMMERCIAL LAUNCH COSTS TO ORBIT [38]

LAUNCHER	LBS TO LEO	PER LB MIN/MAX PAY.COSTS	GEOSYNCHRONOUS TRANSFER ORBIT		
Proton	44,200	$1697/$2149	Proton	10,150	$7389/$9360
Ariane 5	39,600	$3788/$4545	Ariane 5	15,000	$10,000/$12,000
Sea Launch	35,000	$2143/$2714	Sea Launch	11,050	$6787/$8597
Zenit 2	30,000	$1167/$1667	Ariane 4	10,900	$9174/$11,468
LM-3B	29,900	$1672/$2341	LM-3B	09,900	$5051/$7071
Ariane 4	21,000	$4762/$5952	Delta 3	08,400	$8929/$10,714
Atlas 2	19,050	$4724/$5512	Atlas 2	08,200	$10,976/$12,805
Delta 3	18,280	$4103/$4923	Delta 2	04,060	$11,084/$13,547
Soyuz	5,400	$2273/$2597	LM-2C	02,200	$9091/$11,364
Delta 2	11,220	$4011/$4902	Taurus	01,290	$13,953/$15,504
LM-2C	7,040	$2841/$3551	**Average Cost-per-LB to GTO: $9,243/$11,243**		
Athena	04,350	$5057/$5977			
Rockot	04,100	$2927/$3659			
Taurus	03,100	$5806/$6452			
Pegasus	03,300	$3636/$4545			
START	01,543	$3240/$6481			
Average Cost-per-LB to LEO: $3632-$4587					

Since the areal density of a mirror is defined using the thickness of the material used, you simply cannot compare the areal density of a mirror fabricated by ultra-low expansion glass to the areal density of a membrane mirror created out of polyvinylidene fluoride (PVDF). This is because the minimum thickness of the each mirror is determined by the structural integrity of the material being used. Therefore, in order to achieve a true comparison, we have to use the system areal density. The system areal density is defined as the mass per surface area for an optical structure, as defined in Equation (2.1) where ρ is the density of the material, h is the height, V is the volume and, m is the mass.

$$\rho_{areal} = \rho h = (m/V)\, h \tag{2.1}$$

This literature review will cover three areas 1) mirror fabrication, 2) mirror actuation, and 3) control algorithms with a focus on potential for future space based applications. For a comprehensive review of membrane mirrors please review "Lightweight Dynamic In-Plane Actuated Deformable Mirrors for Space Telescopes," by M. Shepherd [30]. Membrane mirrors and fabrication techniques vary widely, so this section is broken down into materials and different construction techniques. Actuation methods also vary as much as mirror fabrication techniques, and this review will cover the following actuators: Piezoelectric, Photostrictive, Thermal Actuation, Dielectric Elastomers, and Ionic Electroactive Polymers. Active shape control requires a complex feedback loop and therefore, this review will discuss current mirror model development and active shape control algorithms.

2.2 Mirror Selection and Fabrication

Membrane mirrors have varied uses such as in-expensive lightweight replacements for traditional large optics or future space based applications. As defined by Hardy, membrane mirrors have no inherent stiffness, so that tension must be applied to maintain a flat surface. Very small forces are required to displace a membrane, and deflection is usually achieved without physical contact, using electrostatic actuators [11]. For this reason the choice of substrate is a crucial first step in the fabrication process. Deciding on a substrate for any given application is not black and white. Each substrate has positives and negatives associated with them and a cost benefit analysis is needed to find the best solution. Furthermore, fabrication techniques vary based on materials used and whether the mirror will be actuated or not. The research herein uses a unimorph structure constructed out of PVDF, however, other materials and fabrication techniques will be explored below.

2.2.1 Materials

In an analysis of low coefficient of thermal expansion (CTE) glass, Silicon Carbide ceramics (SiC) and Beryllium substrates, Roland Geyl and Marc Cayrel [8] defined six key functions that a high performance lightweight mirror substrate should have:

- allow the production of a smooth optical surface leading to highest reflectivity once coated,
- provide maximum stiffness for minimum weight,
- keep achieved optical figure under gravity or mechanical loads,
- lead to high eigenfrequencies,

- keep the optical figure under thermal load and also through time,
- remain at reasonable cost for decreasing area density.

These functions can be applied to either ground or space based applications having large scale optical requirements. In Table 2.2 [28] and Table 2.3 [22] below, the material properties for several lightweight substrates are listed.

Table 2.2 Material Properties of CTE Glass, SiC and Beryllium [28]

Class of material			Ti-doped quartz	LiAlSi-glass-ceramics	Cordierite	SiC	Beryllium
Property	Symb	Unit					
Elastic Modulus	E	[GPa]	67.6	90.3	140	430	307
Density	ρ	[g/cm^3]	2.21	2.53	2.67	3.2	1.844
CTE	A	[10E-6/K]	0.015	0.02	0.02	4.1	11.5
Vickers Hardness		GPa	0.4	4.8	7.2	21.6	2
Mean specific heat	c	[J/(kg*K)]	767	800	730	630	1925
Thermal conductivity	λ	[W/(mK)]	1.31	1.46	4	60	216
Volume resistivity		[Ωcm] @ 20° C	10 [@200° C]		>10^{14}	2*10^3	4.3*10^{-5}
Dielectric constant		[@ 1kHz]	3.99	8.00	4.8 (@ MHz)	-	Metal
Specific stiffness (larger is better)	E/ ρ	[10E6m]	3.1	3.6	5.2	13.4	16.6
Steady state thermal distortion coefficient (larger is better)	λ /α		87	73	200	14	19
Molding			Not possible	not possible	Possible	not possible	Possible
Joint methods			not proven	under test	Proven	not proven	Proven
Milling			Very good	Excellent	Good	Good	very good
Polishability			excellent	very good	Good	Poor	Good
Fracture toughness	KIχ	[MPa]/ [sqrt(m)]	0.70	0.85	1.3	4.9	11

Table 2.3 Material Properties of PVDF [22]

Symbol	Parameter	PVDF	Copolymer	Units
t	Thickness	9, 28, 52, 110	<1 to 1200	μm (micron, 10^{-6})
d_{31}	Piezo Strain Constant	23	11	10^{-12} $\frac{m/m}{V/m}$ or $\frac{C/m^2}{N/m^2}$
d_{33}		-33	-38	
g_{31}	Piezo Stress constant	216	162	10^{-3} $\frac{V/m}{N/m^2}$ or $\frac{m/m}{C/m^2}$
g_{33}		-330	-542	
k_{31}	Electromechanical Coupling Factor	12%	20%	
k_t		14%	25-29%	
C	Capacitance	380 for 28μm	68 for 100μm	pF/cm², @ 1KHz
Y	Young's Modulus	2-4	3-5	10^9 N/m²
V_0	Speed of Sound stretch:	1.5	2.3	10^3 m/s
	Sound thickness:	2.2	2.4	
p	Pyroelectric Coefficient	30	40	10^{-6} C/m² °K
ε	Permittivity	106-113	65-75	10^{-12} F/m
$\varepsilon/\varepsilon_0$	Relative Permittivity	12-13	7-8	
ρ_m	Mass Density	1.78	1.82	10^3kg/m
ρ_e	Volume Resistivity	$>10^{13}$	$>10^{14}$	Ohm meters
R_{T1}	Surface Metallization Resistivity	<3.0	<3.0	Ohms/square for NiAl
R_{T1}		0.1	0.1	Ohms/square for Ag Ink
tan δ,	Loss Tangent	0.02	0.015	@ 1KHz
	Yield Strength	45-55	20-30	10^6 N/m² (stretch axis)
	Temperature Range	-40 to 80...100	-40 to 115...145	°C
	Water Absorption	<0.02	<0.02	% H_2O
	Maximum Operating Voltage	750 (30)	750 (30)	V/mil(V/μm), DC, @ 25°C
	Breakdown Voltage	2000 (80)	2000 (80)	V/mil(V/μm), DC, @ 25°C

LiAlSi-glass-ceramics, Cordierite, SiC, and Beryllium are all currently being explored for large scale ground based applications. PVDF is currently being explored for space based applications because of its low molecular density, ability to be stored in a compact state without degradation, and shape control properties. From Tables 2.2 and 2.3 above, it can be seen that the density of PVDF is lower then that of LiAlSi-glass-ceramics, Cordierite, SiC, and Beryllium. Furthermore, when PVDF is poled (subject to high electric field), a piezoelectric effect is created that can cause a piston effect on the surface. This is a very attractive property which has enormous weight savings

considering other alternative actuation methods, as discussed in Section 2.3 below. These attributes lead to the choice of PVDF for our research. One detractor is that there is a loss on weight savings indicated in Table 2.2 due to the optical coatings that need to be placed on the substrate, unlike glass that can be ground down and polished.

2.2.2 Mirror Fabrication

A study done at the University of Arizona [3], explores conditions for flat membrane mirrors which can be used to define requirements for un-actuated membrane mirrors. It states that a simple stretched membrane will be flat as long as the following conditions are met. First, the perimeter must be in a plane. Second, positive tension must be maintained; the membrane will buckle and wrinkle in compression. Third, the membrane must have uniform thickness. The surface variation will be half as large as thickness variations. Finally, the membrane must be isolated from external disturbances.

One of the simplest methods for creating a membrane mirror, the Duel Anamorphic Reflector Telescope (DART) precision test bed currently employs two tensioned copper foil membranes for reflective surfaces. These membranes are shaped into cylindrical parabolas by incrementally increasing the tension at the boundary until it reaches 40 pounds of tension. The membranes are then held in tension for the life of the mirror [1].

Un-actuated membrane mirrors, flat or curved, are not well suited for space based applications. During the course of a spacecrafts' life span it will experience disturbances such as structural vibrations that prohibit an un-actuated mirror from remaining flat. Actuation of large scale membrane mirrors is absolutely necessary in the space environment to maintain shape control. However, the technology is not mature enough to demonstrate large scale control, so current work is being done to demonstrate control on meter or less sized membrane mirrors.

Work currently being done by Marker, deBlonk, Patrick, Moore, and Chodimella [25] on a meter-class (0.7m) actively controlled membrane mirror begins by tensioning a CP1-DE substrate around a ceramic ring. Active boundary control comes from pressure created by 18 electrostatic actuators located circumferentially around the outer 1 inch of the membrane outer diameter coupled with 32 out-of-plane normal actuators. The weight savings gained by using a membrane substrate are subsequently lost because of the weight gained due to the number of external actuators attached to the mirror and electronics needed for their actuation scheme.

Work done at JPL [44] focused on developing a microelectromechanical system (MEMS) deformable membrane mirror. The proposed system used a single crystal silicon (SCS) continuous backed by an array of electrostatic actuators with corrugated membranes. The mirror membrane deflects downward by the pulling force of the underlying electrostatic actuators.

Research completed at the Air Force Institute of Technology (AFIT) [33] has used a circular piezoelectric in-plane actuated unimorph deformable mirror constructed out of PVDF that has been stretched in tension across and aluminum ring (inner diameter 5",

outer diameter 6") using epoxy. The nickel/copper-coated PVDF membranes were then etched with an electrode control pattern to enable actuation of specific regions of the mirrors. The optical surfaces were created by pouring silicone rubber over the controllable substrates to produce flat, semi-reflective surfaces. This is done by spinning the excess silicone rubber off as it dries. The mirror was coated with a layer of gold or silver to enhance reflectivity.

With weight savings for the entire system being the primary goal for membrane mirror design, meaning not only does the density of the material used need to be accounted for but actuation methods must be considered as well. While membrane mirrors constructed out of materials such as beryllium or created with MEMs technology provide a significant weight savings over traditional large scale optics, that savings is reduced by the electronics and hardware needed for surface actuation. For this reason PVDF is an attractive material because of its inherent piezoelectric properties. The next section will discuss piezoelectric actuators as well as other alternative actuation methods.

2.3 Actuation Methods

This research focuses on actuation using piezoelectric materials. However, there are other alternatives being explored to achieve in-plane actuation such as thermal, photorestrictive, dielectric elastomers, and ionic electroactive polymer actuators. These actuation methods are taken from Shepherd [30] citing his references with a summary at the end of the section discussing why PVDF was chosen for this research.

2.3.1 Piezoelectric

In terms of the maturity of the technology piezoelectric actuators currently are the best solution for in-plane actuation for space based applications. According to the text by

Hardy the direct piezoelectric effect is the creation of an electric charge in a material under an applied stress [10]. Piezoelectric materials have the ability to hold a constant strain under an applied current. These materials may be ceramic- or polymer-based, along with naturally occurring quartz and other crystals. Ceramic-based piezoelectric material largely are directional, due to a process called poling, where the piezoelectric properties are strengthened by applying an electric field at high temperatures, leaving a residual polarization [17]. Steel, Harrison and Harper explored piezoelectric ceramic lead zirconate titanate (PZT) as an in-plane actuator, including the directional effects of poling, hysteresis, and strain [35]. Steinhaus and Lipson created a PZT forced deformable plate mirror [36].

Polyvinylidene fluoride (PVDF) is the primary material being used at AFIT as an actuator for a deformable mirror [42, 43, 33, 34, 18, 40, 26] and Sandia National Laboratories[37]. Polymer-based piezoelectric actuators generally require much greater voltages than ceramic-based actuators [2]. Work is being done by Sessler and Berraissoul [29] to increase the strain rates available from PVDF through excitation by electrons during the poling process. Dargaville et al [5] is also working to space qualify PVDF material.

A significant enabling technology for the use of piezoelectric actuators on the in-plane actuated deformable mirror is electron gun control of the piezoelectric actuator, as demonstrated by researchers at the University of Kentucky [20, 9, 23, 10]. By using an electron beam to charge the electrode field of the piezoelectric actuators, wiring to the individual electrodes is eliminated. In a space application, one could have a single beam generator to control the system that is not attached to the mirror structure itself except for

the ground electrode, simplifying and isolating the mirror structure and control system. Unfortunately, the strain response has shown to be non-linear as the speed and predictability of the strain differs depending on positive or negative control voltage. For positive voltage, the results are predictable and fast, however for negative voltages, the time response increases and precision decreases [9, 10]. The most recent published experimental results for electron gun piezoelectric actuation were from Choi et al at the NASA Langley Research Center and Norfolk State University who demonstrated piezoelectric static actuation of a unimorph membrane with voltages up to 230V using 18 Watt X-band microwave drivers 1.8 meters from the membrane [4] in 2004.

2.3.2 Photostrictive

Photostrictive actuators convert high energy light, into mechanical strain energy. Shih and Tzou [32] and Shih, Smith, and Tzou [31] modeled smart structures with photostrictive actuation. The compound exhibiting the photostrictive behavior was PLZT, composed of lead (Pb), lanthanum (La), zirconium (Zr) and titanium (Ti). The primary advantage of such an actuator would be the non-contacting nature of the control input (light) without the need for individual electrodes as is the case for piezoelectric material. Similar to the electron gun control of the piezoelectric actuator, photostrictive actuators could have a significant impact on large scale (tens of meters) space-based optics where the number of actuators and associated hardware needed to control the mirror would significantly increase the mass of the structure.

2.3.3 Thermal Actuation

There has been very little investigation into thermal actuation. Das et al [6] states that a shape memory alloy is an alloy material that may be deformed at a low

temperature, and upon heating returns to its original state. Investigating thermal actuation to deploy a membrane mirror Pollard and Jenkins [27] noted that the binary (2-phase) nature of the material makes it impractical to use for fine surface control, plus shape memory alloys suffer the same temperature control liability as thermal actuation. Control could theoretically be applied with a heat load using any material with a coefficient of thermal expansion. Slow time constants, the rate difference of heating and cooling, and difficulty in maintain a temperature field in the space environment limit this as an actuation method for high bandwidth, high precision requirements.

2.3.4 Dielectric Elastomers

According to Madden [19] dilelectric elastomers are described as two metallic plates, which are positively attracted to each other in the presence of an electric field, and are used to sandwich a layer of a dielectric polymer such as silicone. When a voltage is applied, the plates compress the dielectric with a pressure proportional to the relative permittivity and free space permittivity and the square of the quantity of voltage divided by the spacing of the electrodes. Assuming the layer is incompressible, the dielectric polymer material displaces in the axial directions. The downside to dialectric elastomers are the high voltages required for thick polymer layers and its reliance on incompressible materials for actuation. For instance, a silicone-based dielectric elastomer actuator is limited from -100^{o}C to 250^{o}C [19]. The current need for high voltages and operating temperatures in this range do not make dielectric actuators a good fit for space applications.

2.3.5 Ionic Electroactive Polymers

Ionic Electroactive Polymers (EAP), such as Carbon Nanotubes, Conductive Polymers (CP), and Ionic Polymer Metallic Composites (IPMC) produce a strain by a redistribution of ions from oppositely charged electrodes transported via a conducting electrolyte [19]. When placed under a voltage potential, cations in a polymer matrix immediately swell clusters on the side nearest the negative electrode (cathode), and shrink on the side nearest the positive electrode (anode). Over time, the pressure gradient in the structure replaces the lost volume of positively-charged ions (cation) with a similar amount of liquid, until equilibrium is achieved. All materials at present require a liquid electrolyte to operate [24], this limitation needs be overcome for space applications. Individual material flaws include high current requirements for CP, poor efficiencies for Carbon Nanotubes, and inability to maintain a steady-state strain for Ionic Polymer Metallic Composites [19, 41].

When considering which actuation method to implement, all of those listed provide positives and negatives. The most important attributes to consider are functionality and weight savings. Issues that limit the choice of several action methods include:

- Piezoelectric
    - Non-linear strain response at high speeds
- Photorestrictive
    - High-energy light source needed
- Thermal

    - Slow time constants, the rate difference of heating and cooling, and difficulty in maintain a temperature field in the space environment limit this as an actuation method for high bandwidth, high precision requirements
- Dielectric Elastomers
    - High voltage needs
- Ionic Electroactive Polymers
    - High current needs

Based on these negative attributes as well as current technological maturities, piezoelectric actuators were chosen for this research. However, for future large scale actuation will require numerous actuators and this method will also lose significant weight savings. As technologies mature, the electron gun method of actuating a piezoelectric actuator seems to be the most weight efficient method of actuation.

2.4 Control Algorithms

Implementation of actuators on deformable mirrors in general have been studied at large and it has been determined that an algorithm that utilizes influence functions (IFS) is the best method for control. Actuator IFS describe the deformed surface shape that results from a force applied by the actuators. These surface deflections are measured by a wavefront sensor which then calculates a defined number of Zernike polynomials which represent the modal shapes of the surface. Hardy defines Zernike polynomials as a set of orthogonal polynomials that arise in the expansion of a wavefront function for optical systems with circular pupils [11]. Figures 4.1 through 4.7 below are three dimensional representations of the first 7 Zernike coefficients simulated in Matlab.

Active quasi-static shape control of circular apertures to produce Zernike polynomial surfaces has been investigated by more than one researcher. Zernike polynomials will have some displacement at their boundary, as long as membrane structures envisioned in this application are characterized by a fixed, non-displacing, boundary[30]. In order to achieve closed-loop control, a controller matrix based on the IFS is created. Measured wavefront error is corrected with actuator commands determined by the controller matrix in a closed feedback loop.

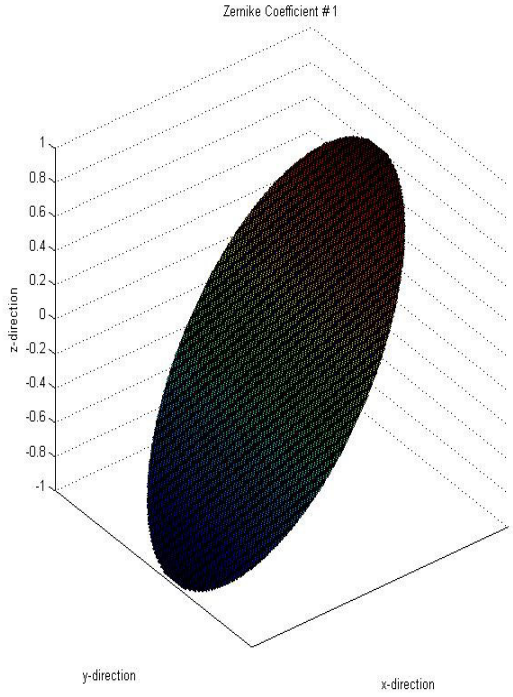

Figure 2.1 Zernike Coefficient #1 (Matlab)

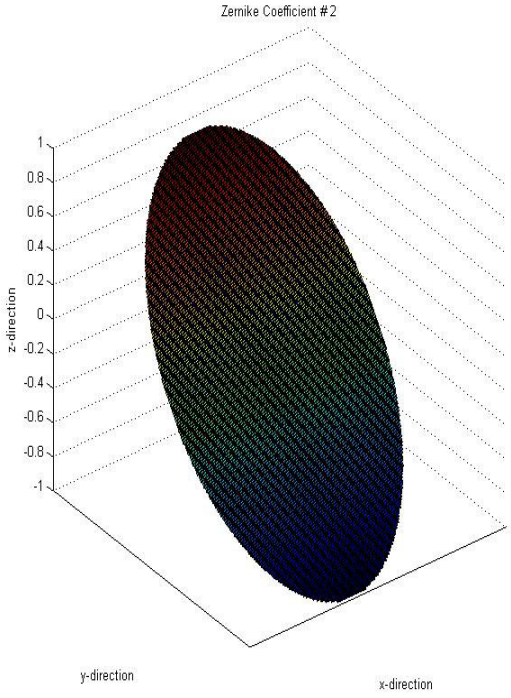

Figure 2.2 Zernike Coefficient #2 (Matlab)

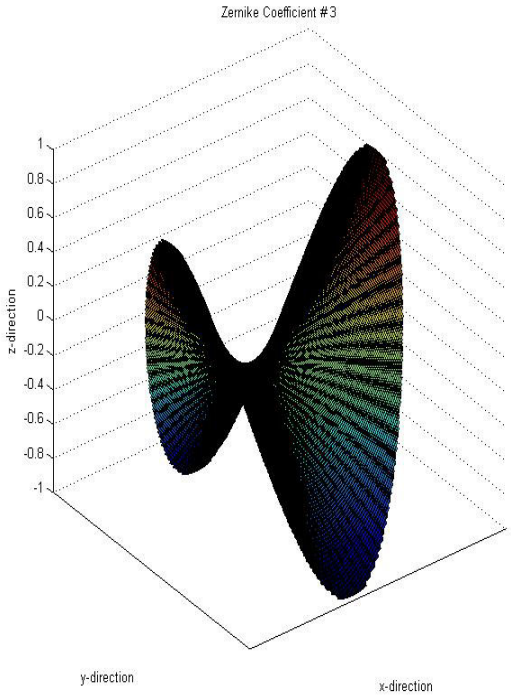

Figure 2.3 Zernike Coefficient #3 (Matlab)

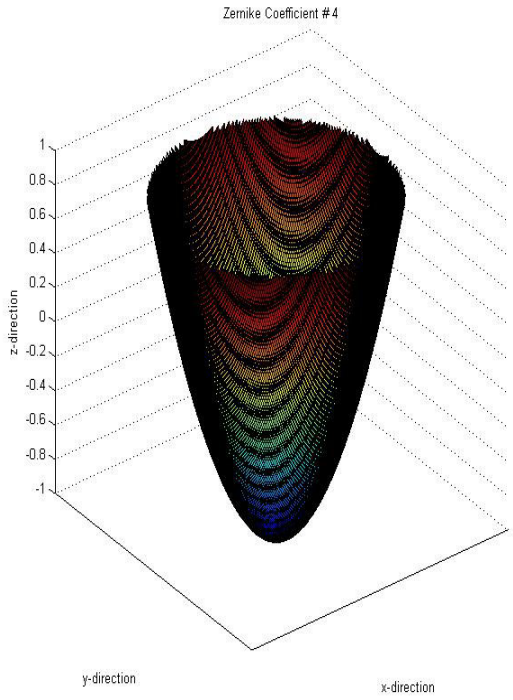

Figure 2.4 Zernike Coefficient #4 (Matlab)

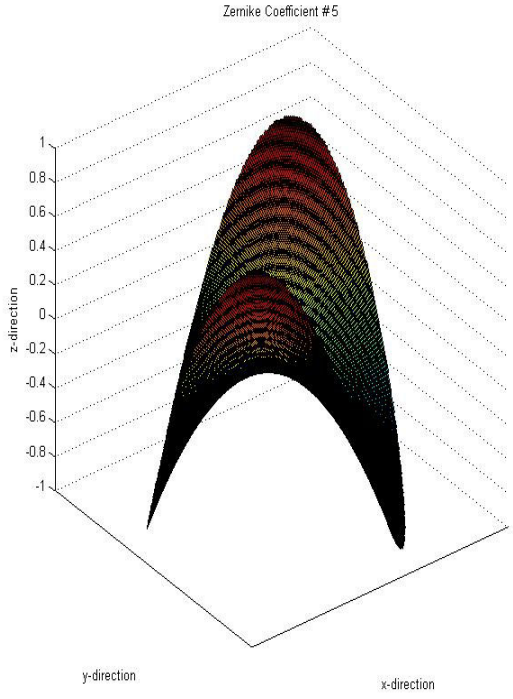

Figure 2.5 Zernike Coefficient #5 (Matlab)

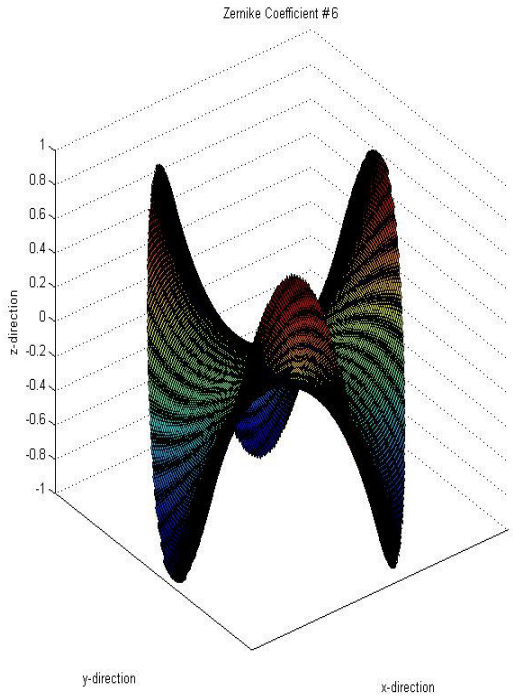

Figure 2.6 Zernike Coefficient #6 (Matlab)

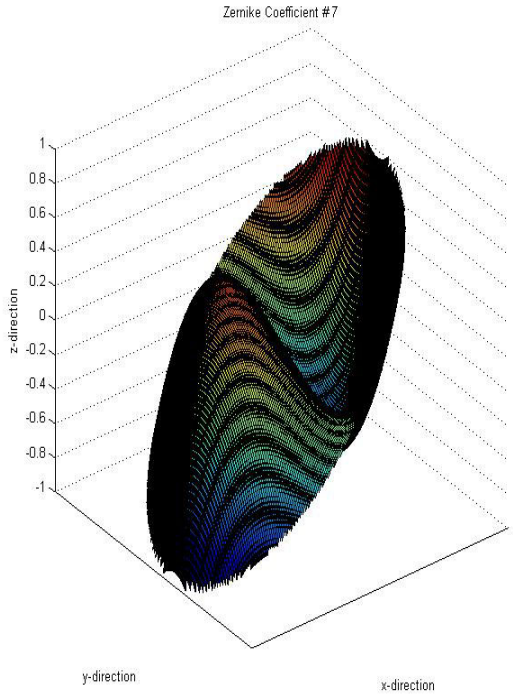

Figure 2.7 Zernike Coefficient #7 (Matlab)

2.4.1 Modeling

Derivations begin with the complexity of the mirror model. A simple model assumes each actuator is a point force acting like a spring attached to a rigid reaction structure. Research done by Thorburn and Kaplan used a control matrix derived from experimentally measured IFS demonstrated a 50 percent improvement in surface quality through an iterative process where new actuator commands were determined from the measured wavefront error and control matrix for a 97-actuator conventional deformable mirror [39]. In another study by Menikoff, the actuator IFS are analytically derived for a circular plate by a Fourier series expansion. They are found to be similar to traditional finite-element analysis [21]. The influence function shapes from the finite element model are compared to experimentally measured shapes. A model created in a study done by Hiddleston, analytically determined shapes reduced execution times significantly and eliminate peculiarities that show up in the actual surface [12].

A more complex analytic derivation achieves a nonlinear feedback controller by first determining nonlinear IFS. The modal non-interaction control represents the ability to control the amplitude of individual modes as long as the displacement at each actuator can be measured. The derivation uses a linear approximation when surface displacements are much less then the mirror thickness. This derivation was done for circular, deformable, electrostatic, membrane mirrors with modal representation by Zernike polynomials [44].

Influence functions are not the only method for actuation control but an in depth analysis of other methods will not be provided here. One conceptual control algorithm

assumes a future structure with built-in actuators, sensors, and computational elements requiring only local error information and actuator capability knowledge [7].

2.4.2 Active Quasi-Static Shape Control

Wang and Hadaegh [45] presented the problem of surface control for a circular deformable mirror in terms of the orthogonal basis set, and provide an example where a circular membrane mirror is controlled by electrostatic actuators to form the axisymmetric Zernike shapes. However, the methods are limited to those shapes where the boundary condition may be imposed, but do provide a methodology for actuating a surface in modal coordinates. Forming Zernike shapes on electrostatic membrane mirrors (mirrors that are forced by electrostatic attraction between electrode pairs on the mirror and a backing plate) has long relied on iterative techniques, fittings, and calibration curves. Claflin and Bareket [30] published the basic least squares fitting technique in 1986. The solution methodology of using numerical solutions to Poisson's equation (the governing equation for membrane structures) with an unused “transition zone" between the measured interior area and the fixed membrane boundary show the difficulty of using membrane mirrors to make Zernike shapes.

Modal shape control using Zernike polynomials has been studied in depth at AFIT and it has been shown that modal shape control and error correction are possible in a quasi-static closed-loop system by implementing control based on IFS. Based on this success, this research will endeavor to implement an IFS controller to demonstrate error correction and modal shape control in a dynamic closed-loop system.

III. Mirror Construction and Test Setup

3.1 Overview

New mirror fabrication processes and a new data acquisition system (DAS) have been implemented in regard to previous research in this field done at AFIT. The focus of this chapter is to illustrate how the membrane mirror is constructed out of PVDF and its evolution from previous mirrors. Furthermore, this chapter will discuss changes to the data acquisition system at AFIT from previous research.

3.2 Mirror Construction

Previous research conducted at AFIT has resulted in fabrication techniques that have shown global shape control over a membrane mirror surface [33]. This process consists of using a stretched PVDF membrane etched with seven actuation patches bonded to an aluminum ring (see Figure 3.1). The membrane mirror fabrication process is an iterative process which continues to evolve. Lessons learned from previous iterations include 1) the electrode tabs provided too much stress and led to cracking in the electrode, 2) mounting issues present by using a ring configuration and 3) a lack of tilt control. This research addresses these lessons learned, creating another iteration to the evolving membrane mirror fabrication process.

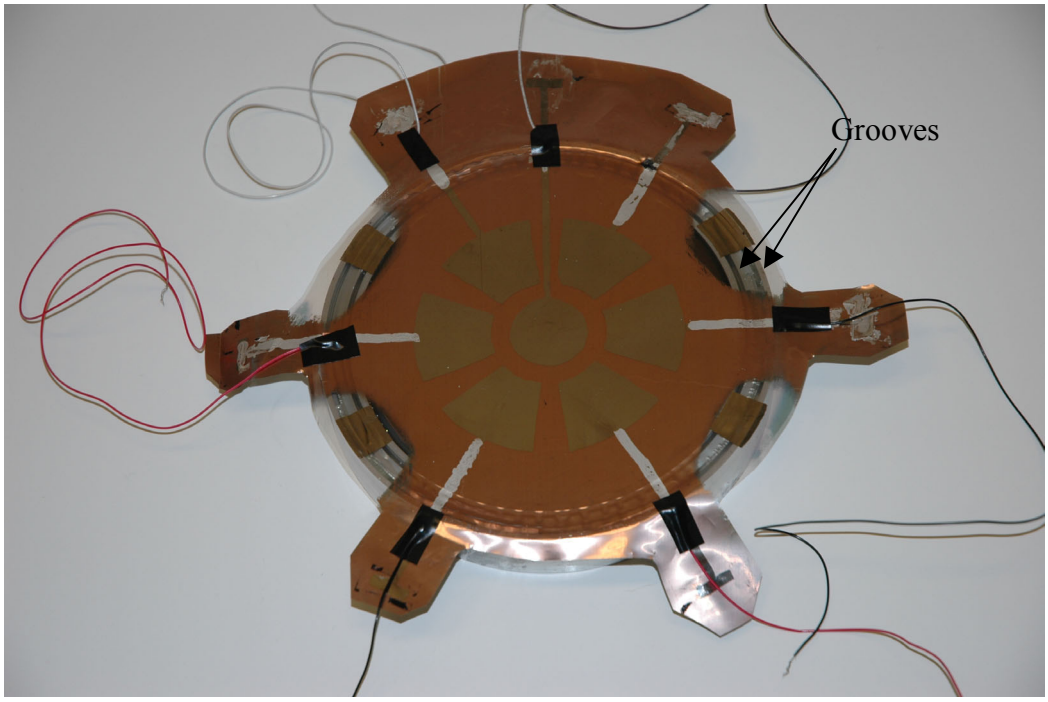

Figure 3.1 Previously Fabricated Membrane Mirror

3.2.1 Aluminum Ring Design

The previous design for the aluminum ring was 6" diameter (5" inner diameter) and approximately ¾" thick. The mounting surface had two grooves that spanned the entire surface to ensure that enough epoxy was present for a good bond between the ring and the PVDF. Several holes were drilled into the bottom surface to allow for mounting. Analysis of this design after the last mirror was fabricated confirmed that the two groves were unnecessary. Furthermore, the current method for mounting needed to be improved for better alignments as well as to allow the ability to correct for the decorrelation of the wavefront due to the errors in pointing relative to the reference, also known as angular anisoplanatism [11].

The new design (see Figure 3.2) retains the proportions from the previous design including being fabricated out of aluminum, and the outer and inner diameters and thickness were held constant. One of the changes was to eliminate the two grooves from

the mounting surface. The function of the grooves (Figure 3.1) was to provide more epoxy to create a bond between the ring and PVDF. The other major change was to insert four equidistantly placed aluminum dowels that were approximately 1" length and 0.25" in diameter around the perimeter of the ring. These dowels will allow for better alignments and should aid in tilt correction in both the x and y axes.

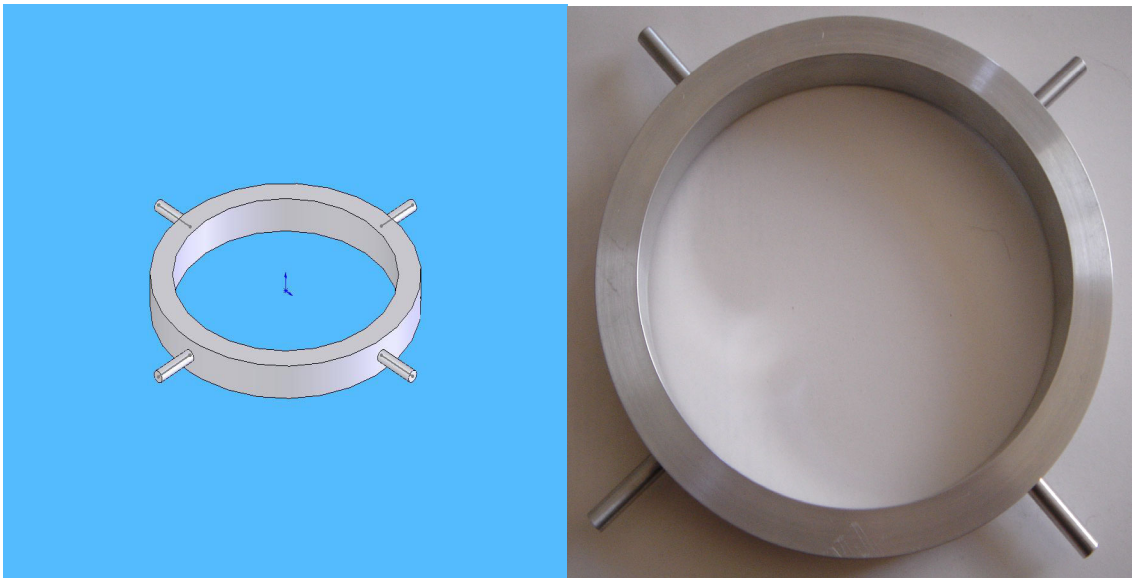

Figure 3.2 Representation of New Aluminum Ring (SolidWorks | Fabricated)

3.2.2 Mirror Fabrication

The membrane mirror was constructed using techniques previously developed at AFIT by Sobers [33]. The PVDF membrane was 52m. A membrane stretching and mounting system was used to keep the membrane under tension while the new 6" diameter aluminum ring was bonded to the membrane using epoxy. The stretching system consisted of a 14" diameter aluminum ring with a rubber o-ring attached, an aluminum faceplate, and four bar clamps. The PVDF membrane was placed between the o-ring and the faceplate. The bar clamps were tightened incrementally until the membrane was taut. A five-minute epoxy was applied to the 6" aluminum mounting

ring, which was then bonded to the membrane. A 0.5" thick aluminum disk was placed on top of the ring along with a 1 lb. weight to ensure a good bond between the membrane and the ring, Figure 3.3. After the epoxy had thoroughly cured, the clamps were loosened and all of the excess membrane was cut away from the mounting ring.

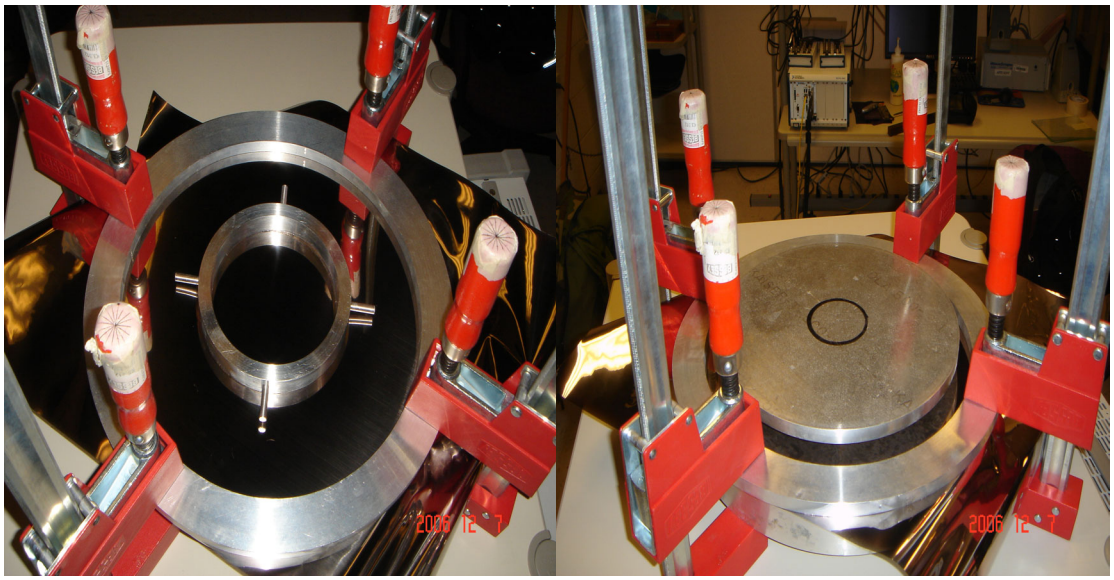

Figure 3.3 Mirror Fabrication (Tensioning)

Originally, the control pattern was applied by first creating a full-size template and then printing it on stiff photographic paper. The electrode sections were then removed using a razor blade, and the electrodes were drawn on the PVDF with a Sharpie marker using the template as a guide. Once the electrodes were drawn with the protective marker, the nickel-copper layer surrounding them was removed using a Q-tip dipped in Ferric Chloride. Thus, the electrodes were electrically isolated from each other and from the back surface, which was used for grounding the membrane. The Ferric Chloride residue was then removed using damp cotton balls, taking care not to use too much pressure when wiping the surface. Once all of the etchant had been cleaned from the membrane surface, the permanent marker covering the electrodes was removed with

cotton balls saturated with isopropyl alcohol. After the electrodes had been etched, the metal on the reverse of the membrane was removed behind the leads so that a charge applied to a particular electrode would not produce a piezoelectric effect along the lead as well.

In a deviation from the original process, after successfully bonding the membrane to the aluminum ring and cutting away any excess membrane. Then the control surface is etched with Ferric Chloride. The surface bonded to the aluminum needs to remain un-etched to ensure that the PVDF is uniformly grounded to the aluminum ring. Then using the aluminum template in Figure 3.4, gold or silver is evaporated onto the etched control surface. According to the manufacturers of the PVDF, Measurement Specialties, gold, copper or silver can be used for the electrode pattern [22].

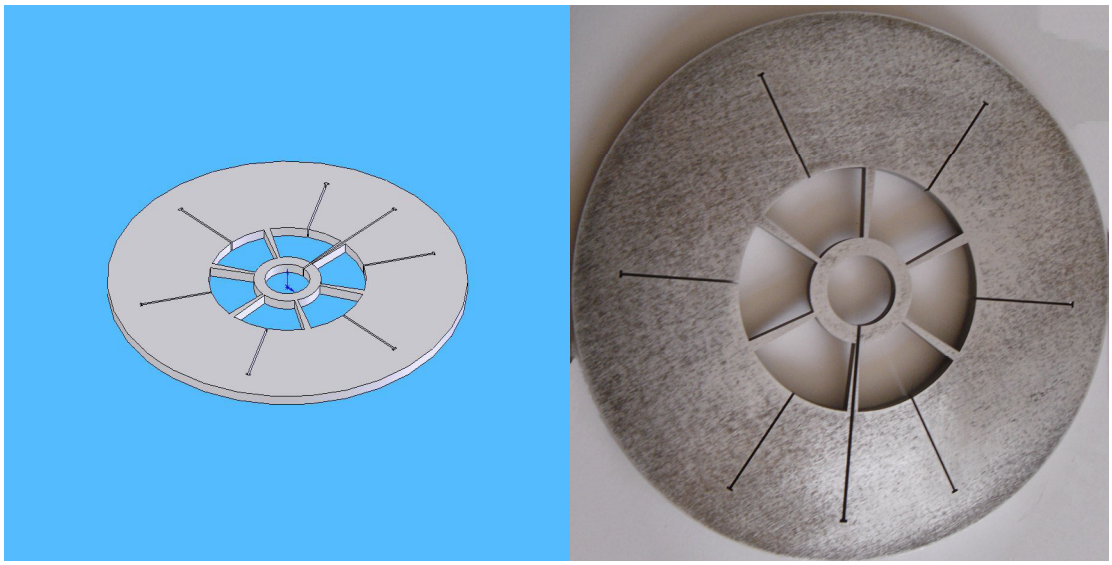

Figure 3.4 Evaporation Template (SolidWorks | Fabricated)

The optical surface was then created by pouring silicone rubber over the controllable substrate to produce a flat, semi-reflective surface. This is done by spinning the excess silicone rubber off as the silicone cures. At this point the mirror can be coated with a layer of gold to enhance its reflectivity. However, the decision was made not to

coat the mirror with gold or silver because the coating has the potential to create an over-damped surface preventing Wavescope from detecting any strains.

The final step in the mirror fabrication is to attach wires to the electrodes and ground. The wires can be attached to the electrode using conductive glue or another conductive material such as conductive copper tape.

3.2.3 Fabrication Results

A new mirror was fabricated with the implemented changes discussed above. Initially the resulting mirror met all expectations. After changing the optical set-up the non-reflective surface was able to reflect enough light to the Wavescope sensor to allow for a full calibration. Furthermore, capacitance checks across all of the actuators showed uniform capacitance of 1.2 nano farads (nf). A significant problem arose when -600 Volts was applied to the second actuation patch. It was determined that the location of the end of the electrode relative to the edge of the aluminum ring was short enough to allow the current to jump that gap and ground itself on the aluminum ring. This caused an electrical fire that burned through the PVDF rendering the second actuation patch permanently inoperable.

Because this did not happen in all seven of the actuation patches two potential reasons have been identified. First, in the process of cutting the excess PVDF from around the ring the edge of the material could have been rounded off exposing a portion of the aluminum ring. Second, etching the PVDF while bonded to the aluminum ring has the potential to weaken the bond between the materials because of the pressure being applied to the surface. It is likely that during the etching process the PVDF could have become separated from the aluminum ring causing a gap that allowed for the grounding.

To correct these potential problems the fabrication process was modified again. The first change was to etch the PVDF prior to bonding the material to the aluminum ring. This will prevent any unnecessary stress from being placed on the epoxy bond. The second change was to allow for approximately 1" of epoxy to be left around the edge of the mirror which will prevent any rounding or cutting issues and will provide enough of a distance for localized grounding not to occur. After using the damaged mirror to demonstrate the system throughput using the unaffected actuators the damaged mirror was disassembled and a new mirror was fabricated but due to the length of time the total fabrication process takes, it was not used to demonstrate closed-loop control.

3.3 Optical Test Setup

Correct optical alignments are crucial to ensuring that the measured Zernike coefficients are accurate. The optical test setup had remained constant throughout the evolution of testing membrane mirrors at AFIT. Sobers [33, 34] and Peterson [26] both document the optical setup of the test bed with its most important features identified below, shown in Figure 3.5. The only deviation from this step-up comes from removing a filter wheel from the beginning of the path and placing it right in from of the λ/20 flat mirror used for the reference signal. This was done to increase the intensity of the laser being reflected off of the target mirror with out a reflective coating while preventing the reference signal from saturating the focal plane array of the Wavescope sensor during calibration.

A 20 mW helium-neon laser (λ = 633 nm) is used to illuminate the test and reference surfaces via a beam splitter. The beam splitter separates the beam into two equal intensity beams. One beam is turned 90 degrees and reflected off a λ/20 flat mirror

to return to the WaveScope WFS-01 Shack-Hartmann Wavefront Sensor (SHWS) manufactured by Adaptive Optics Associates (AOA) as a reference beam. Because the mirror is not coated with a gold or silver coating the reflectivity of the mirror is low and the intensity of the laser must be increased. To compensate for this a filter wheel is placed in front of the λ/20 flat mirror to control the amount of light from the reference signal that reaches the focal plane array. The other beam is passed through the beam splitter, focused with a 1-inch doublet lens, and directed through a variable beam mask. The beam mask is adjusted for each test to illuminate only the desired area of the test mirror. This simplifies test subject area adjustments during calibration. The beam is reflected off the test mirror and returns to the SHWS as a test beam. The test mirror sits in a suspended horizontal position on the optics table, similar to the setup shown in Figure 3.6, by suspending the mirror it allows the mirror to vibrate freely in the frame.

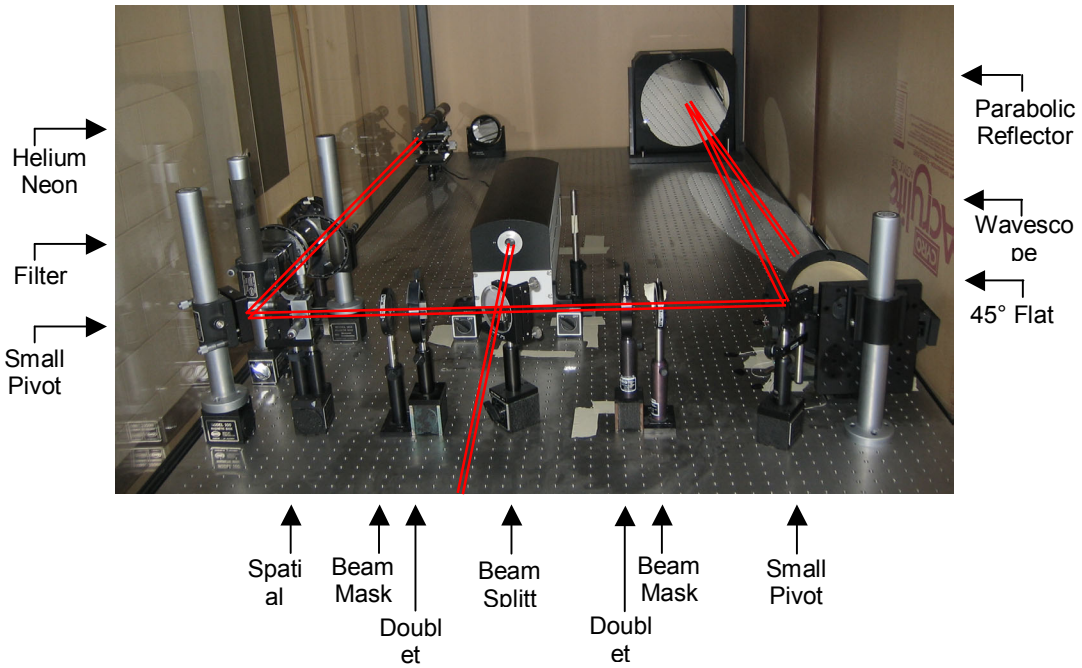

Figure 3.5 Complete Optical Setup

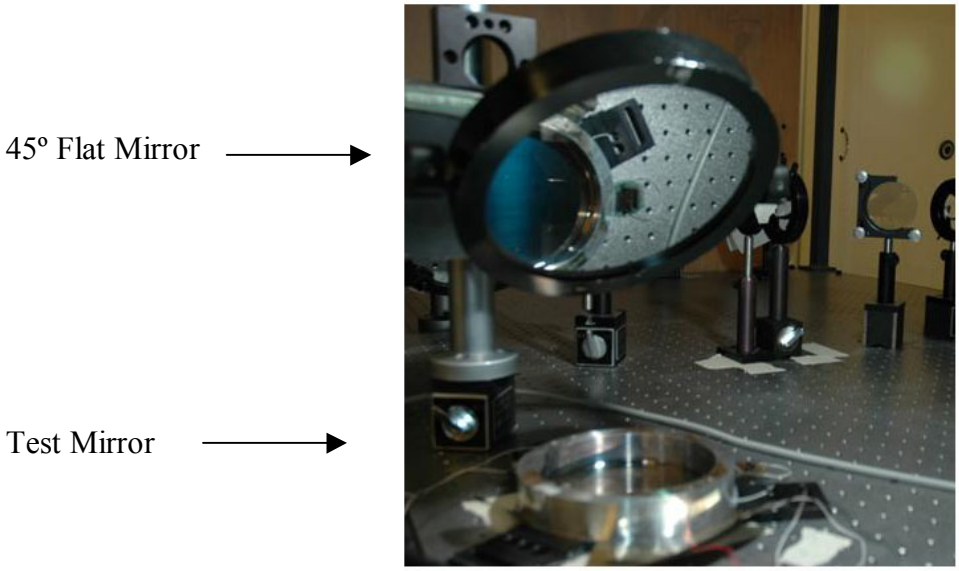

Figure 3.6 Floating Test Mirror

3.4 Wavescope

The Wavescope sensor is a traditional Shack-Hartmann sensor that measures a wavefront and calculates the Zernike coefficients of the mirrors surface. This sensor breaks down a signal into 48x48 sub images that are projected onto a focal plane array using a monolithic lenslet module (MLM). These measurements are extremely sensitive to tilts on the surface being measured, external disturbances, and intensity of the illuminator being used. For this reason the recommended calibration process needs to be used every time data is taken.

3.4.1 Wavescope Calibration

After the deformable mirror is placed in the optical setup, aligned and adjusted to remove tilt, the next step is calibrating the Wavescope sensor to calculate the spot position and pupil size. This ensures that the wavefront measurements are accurate and reliable. This calibration process must be completed any time the optical setup changes, including when the membrane mirror is removed. However, because the Wavescope

sensor is extremely sensitive it is a good idea to perform the full calibration prior to any data collection. The Wavescope software walks you through the calibration process and is briefly discussed below. However the entire calibration process is described in detail in the Wavescope User Manual.

The first step in the calibration process utilizes a uniform light source to calculate a reference signal to ensure that the light illuminates the pixels of the focal plane array correctly. For this research the HeNe laser was split into two paths. The first path was filtered and used as the reference signal. The calibration process can be either completely automated or there is an option to complete this manually. If the automated option is chosen, Wavescope will vary the exposure time for the CCD to regulate the intensity of light introduced to the focal plane array. However, the automated option does not always provide the best light choice for light intensity because of the tolerances that are internally coded. The Wavescope output of the reference signal is shown in Figures 3.7 and Figure 3.8, where every box represents an illuminated pixel. The difference between these two figures is that Figure 3.7 represents a uniform source that is not correctly aligned and does not illuminate the pixels of the focal plane array. After the calibration process is completed the reference signal is no longer needed and should be blocked from the focal plane array.

Once this step is completed Wavescope then repeats the same step for the target signal using the second path from the helium-neon laser. For this research the target signal is the laser return off of the membrane mirror. Figure 3.9 below, is a Wavescope generated plot of the illuminated pixels of the CCD from the Target Signal. This setup is less then ideal with gaps in pixel coverage. This is a direct result of tilt on the mirror and

the position of the mirror needed to be adjusted. Once the intensities and exposure times are set, they cannot be changed otherwise Wavescope will not calculate the Zernike coefficients accurately.

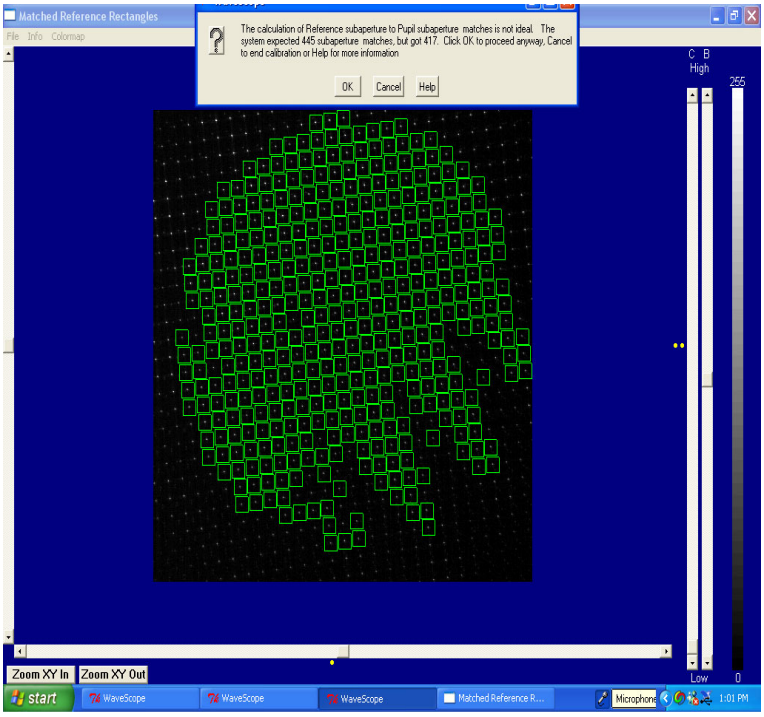

Figure 3.7 Wavescope Calibration of Focal Plane Array Reference Signal (BAD)

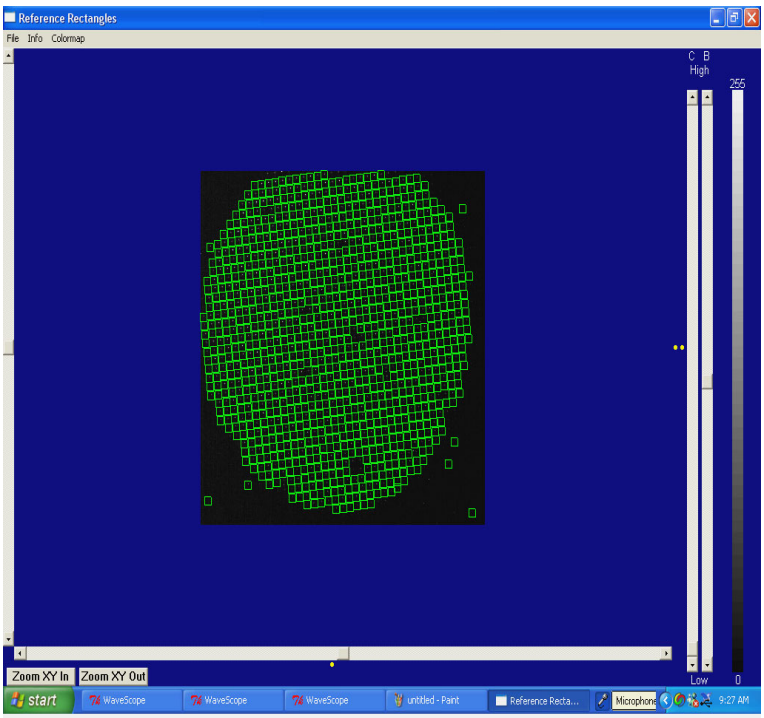

Figure 3.8 Wavescope Calibration of Focal Plane Array Reference Signal

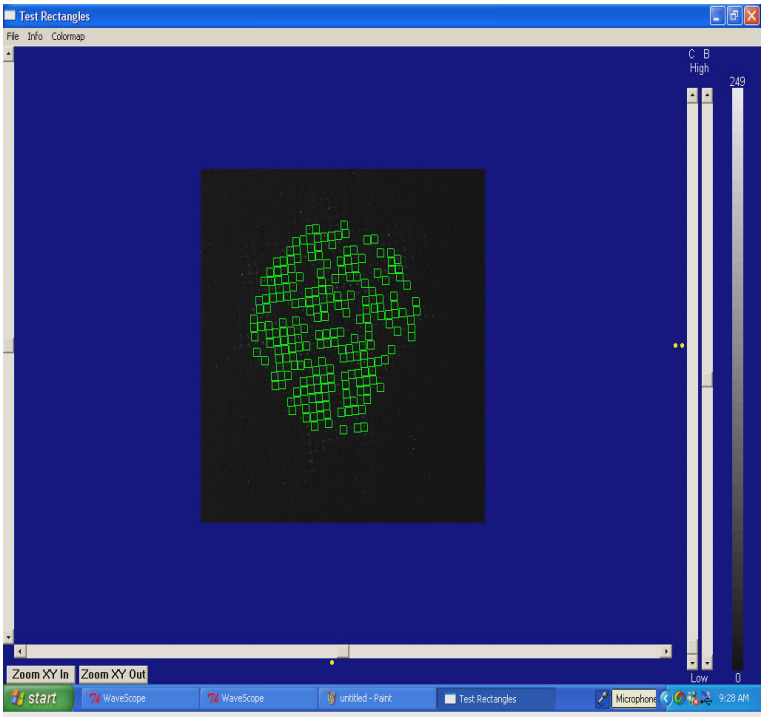

Figure 3.9 Wavescope Calibration of the Target Signal

3.4.2 Wavescope Data Rate

The Wavescope output data rate is determined by three variables, 1) data format, 2) focal plane size, and 3) number of Zernike polynomials outputted. Data can be output from Wavescope in binary or ASCII format. This is done by changing two TCL scripts, socket.tcl and TestEx.tcl, Appendix E. The theoretical output data rates Wavescope can achieve using both ASCII and binary formats are listed in, Table 3.1 [26]. For this research, the ASCII format was chosen outputting 7 Zernike coefficients giving a theoretical data rate of approximately 476 Hz. The actual data rate of 374 Hz doesn't match because of the window size that was selected. A window size of 128 x 128 pixels would provide a data rate close to 476 Hz, however in order to capture enough data to accurately measure deflections on the mirror surface require a window 512 x 512 pixels wide, which reduces the data rate that can be output. However, the limiting factor for the system throughput is parsing the data in Labview.

Table 3.1 Wavescope Data Transfer Rates [26]

Format	# of Coefficients	Byte-Packet	Baud Rate	g	Calculated DR	Determined DR
ASCII	42	1225	1.00E+06	10	82	-
ASCII	36	1051	1.00E+06	10	95	-
ASCII	10	297	1.00E+06	10	337	-
ASCII	7	210	1.00E+06	10	476	50 Hz
ASCII	5	152	1.00E+06	10	658	-
Binary	42	338	1.00E+06	10	296	-

3.5 NI PXI Chassis/Labview

The NI PXI Chassis replaces the D-Space system that was in the data acquisition system. This was done to increase the system throughput in part because the D-Space system read in the Zernike coefficients using an RS232 cable that had a system throughput of 2.5 Hz after several data conversions. In contrast the NI PXI Chassis has a

throughput of approximately 50 Hz. However, by changing the system hardware a change in the programming language used to run tests and control the mirror from Matlabs Simulink to National Instruments Labview was necessary as well.

3.5.1 NI PXI Chassis/Labview Programming

The NI PXI Chassis uses Labview based code to complete any necessary tasks. Similar to Simulink, Labview allows you to build block diagrams called a virtual instrument (VI) that can be used to create individual tasks. Care needs to be exercised when deciding which tasks are performed by a single VI because each VI can only open a connection to one system at a time. The importance of this is if you want to open a connection to read in data from Labview you cannot send calculated voltages to the Chassis with the same VI. For this reason creating a project (Figure 3.9) allows you to link the Wavescope Sensor and NI PXI Chassis by calling separate VIs that work together and share data through common variables. An important note is that the NI PXI Chassis uses digital outputs when creating voltages. This is important because once the code stops generating voltages, the last voltage applied to the mirror will remain on the mirror unless zeroed out or the Chassis is turned off.

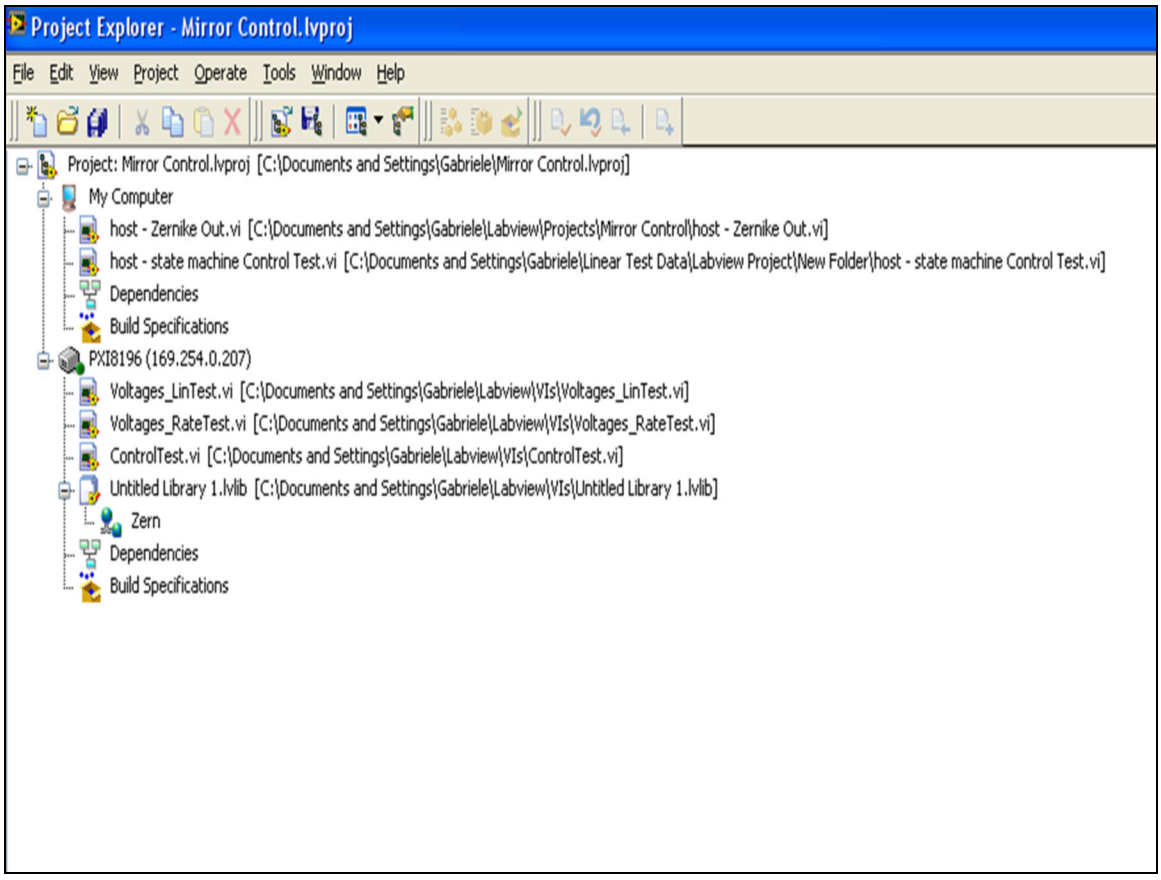

Figure 3.10 Example of a Labview Project

3.5.2 NI PXI Chassis/Labview Data Rate

The throughput of the new data acquisition system is currently not limited by the Chassis but by parsing of data by the Labview software, which is reliant on the amount of data sent in each packet by Wavescope. In the current configuration, Wavescope uses an ASCII data format that sends 7 Zernike coefficients in each data packet, with a size of 210 bytes at a theoretical rate of 54 Hz. Labview creates a TCP connection between the NI PXI Chassis and the Dell computer that is running Wavescope allowing this data transfer. This digital transfer is not always perfect and when an error occurs the TCP link is severed causing an internal error in Wavescope.

In order to ensure that the data acquisition process from data acquisition to voltage generation is uniform, the time it takes to run a single iteration must be fixed. To accomplish this in Labview you need to use the timed-loop feature, this ensures that the same time step was taken between iterations. The timed loop works on a 1 kHz clock that is accurate up to 1 ms, but has the option to work on a MHz clock if the data rate from Wavescope can be improved. For this research, the clock was set to 20 ms (50 Hz), based on the time it takes to read in and parse the data packet from Wavescope, calculate voltages and then send the voltages to another VI where the voltages are generated by the Chassis.

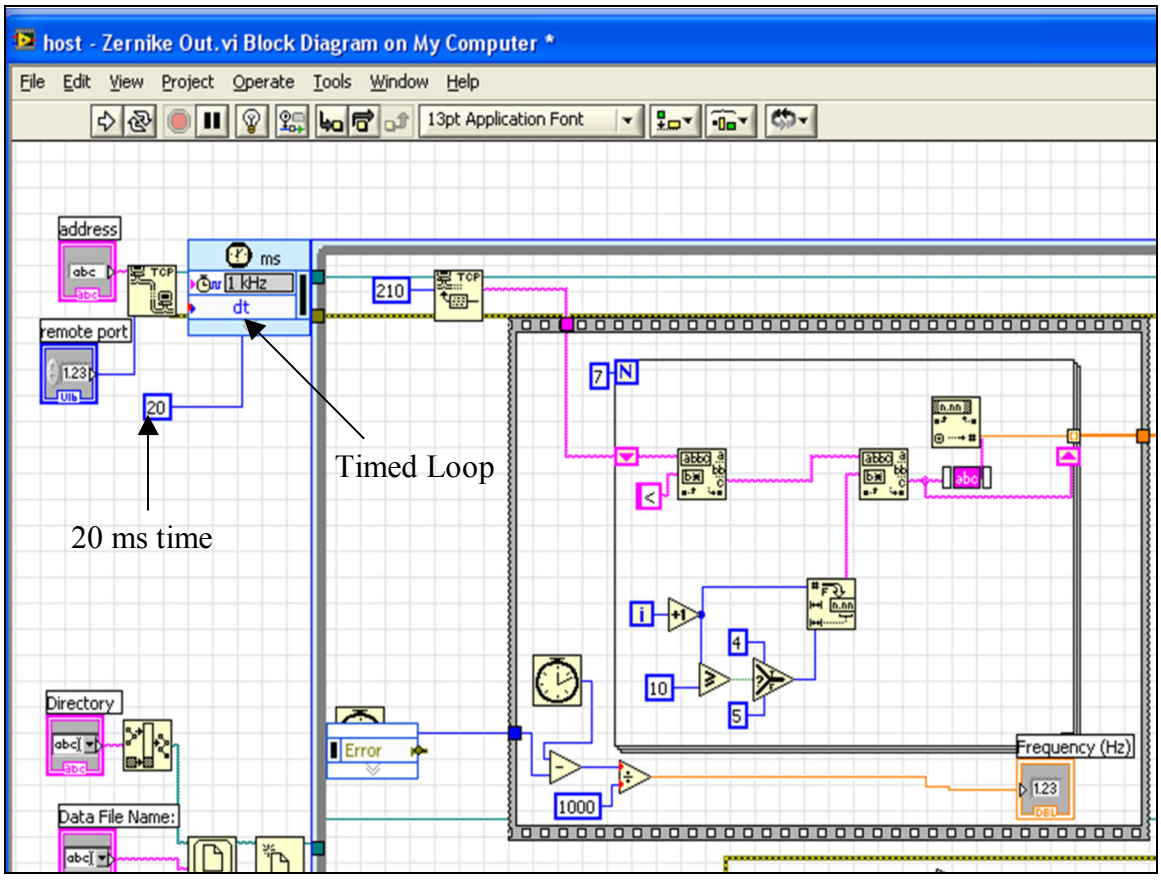

Figure 3.11 Labview Representation of Timed Loop

3.6 Validation of the Data Acquisition System

The previous data acquisition system running at 2.5 Hz limited both the controllability and observability of the system. Switching to the National Instruments PXI Chassis allowed the data transfer rate increase to 50 Hz. While this is a significant improvement to the system throughput, it still does not guarantee that the closed-loop system will be completely controllable or observable due to aliasing at higher frequencies.

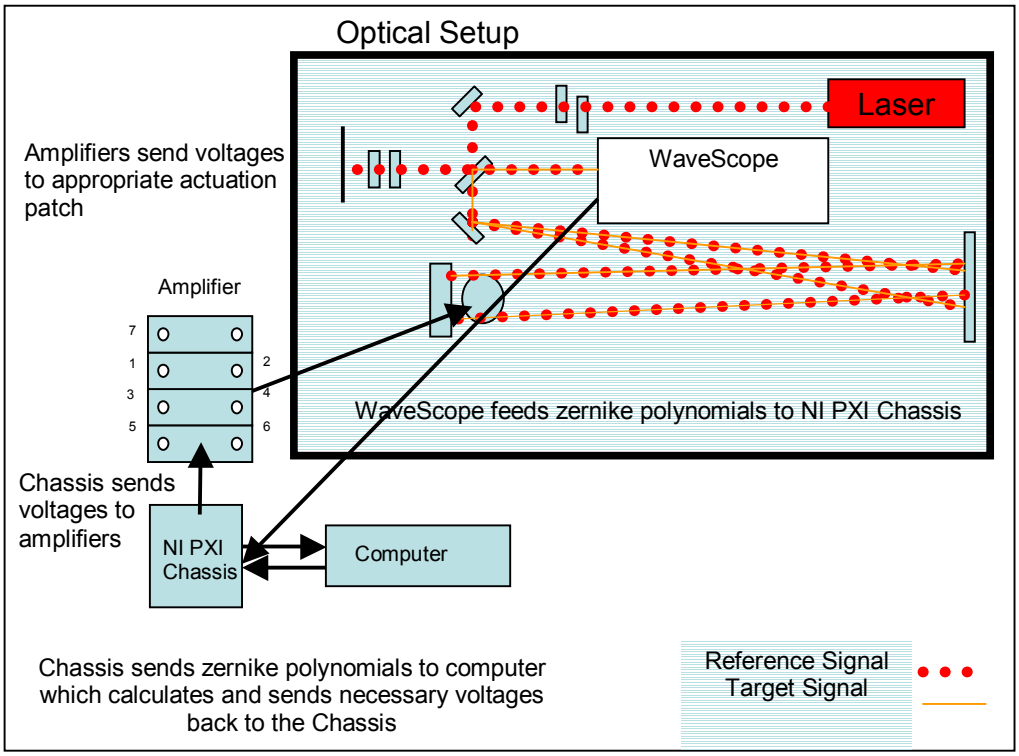

Figure 3.12 Block Diagram of Optical and Data Acquisxition Setup

The Nyquist Criterion states the exact reconstruction of a continuous-time baseband signal from its samples is possible if the signal is bandlimited and the sampling frequency is greater than twice the signal bandwidth. To test that the closed loop process from Zernike measurement through voltages applied to the mirror, system throughput, of the new DAS was actually 50 Hz, a sinusoidal wave was applied to the surface of the mirror on one actuation patch. This wave was created by a signal generator and had maximum amplitude of ±600 volts after being passed through an amplifier. Furthermore, the frequency was varied from 1 Hz to 27 Hz incrementally. A VI in Wavescope was used to capture the Zernike coefficients measured while the sinusoidal signal was applied to the actuator patch. A set of 7x800 data points of the target signal was taken with the Wavescope Sensor before a voltage is applied to the mirror to calculate the "flat" position of the mirror. These 7 sets of 800 data points represent the desired Zernike coefficients

and each set is averaged together to come up with the average starting position for the mirror.

A signal generator was then used to generate a sinusoidal wave with maximum amplitude of 3 V and a frequency between 1 and 27 (Table 3.2), which is then amplified to and amplitude of 600 V before being applied to the mirror. Wavescope, reads in the target signal and calculates the Zernike coefficients based on the modal shape of the mirror and sends that data to Labview (Appendix B.1) which parses the data and writes it to a file.

Table 3.2 Frequency Response Test

# Data Points	Frequency	Amplitude
7x800	0 Hz	0 V
7x800	1 Hz	6 V_{pp}
7x800	5 Hz	6 V_{pp}
7x800	10 Hz	6 V_{pp}
7x800	15 Hz	6 V_{pp}
7x800	20 Hz	6 V_{pp}
7x800	25 Hz	6 V_{pp}
7x800	27 Hz	6 V_{pp}

Figures 3.14 through 3.20 below represent the time and frequency responses of the Zernike coefficients 1 - 3 starting with a 1 Hz and progressing to 27 Hz. It is important to understand that the condition of the mirror was not idea. Due to issues arising with the new fabrication techniques the second actuator caused an electrical fire

that burned a hole through the PVDF, discussed in depth in Chapter III. Because only one mirror was fabricated all of the wires connected to the electrode were removed and reattached closer to the actuation patch on the membrane mirror itself using adhesive copper tape. While this prevented another fire, it also added surface tension to the membrane mirror that has not been previously modeled. This issue directly caused a non-uniform reflective surface on the mirror preventing Wavescope from accurately calibrating the surface, Figure 3.13.

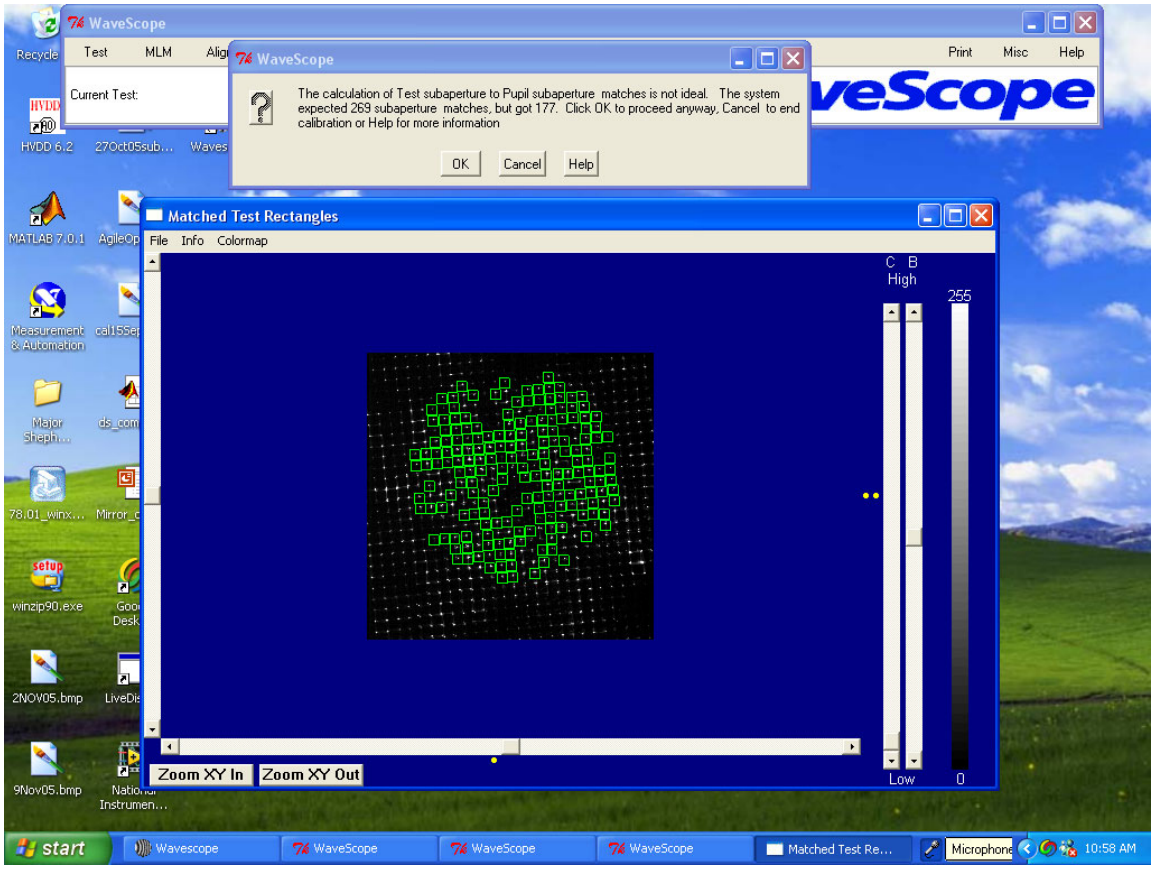

Figure 3.13 Calibration Plot for Rate Tests

Furthermore, the electrodes were deteriorated and while there was a capacitance on the actuation patches it was 0.63 nf or approximately 50% less then a flawless actuation patch. This is a potential cause for noisy time plots (left) and power spectral density

plots, PSD (right), Figures 3.14 - 3.20. However, as the frequency is increased from 1 Hz to 25 Hz, the PSD plots show the maximum power per frequency at the correct frequencies and the time plots match up with an ideal sinusoid of the same frequency. Furthermore, as the frequency is increased above the 25 Hz threshold to 27 Hz, the frequency begins to shift lower to 23 Hz and the time plots are degraded and can be represent by a sinusoid of lower frequency. The plots validate the assumption that in it's current configuration our system is running at 50Hz. This data was analyzed and all plots were generated using Matlab code that can be found in Appendix A.3.

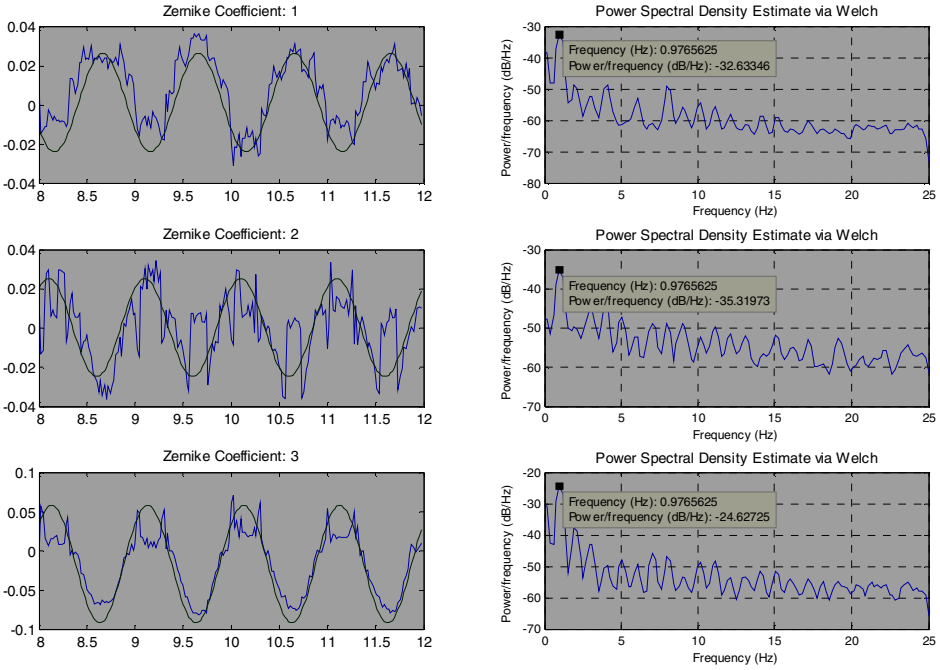

Figure 3.14 Frequency Response 1 Hz (Time Domain/Frequency Domain)

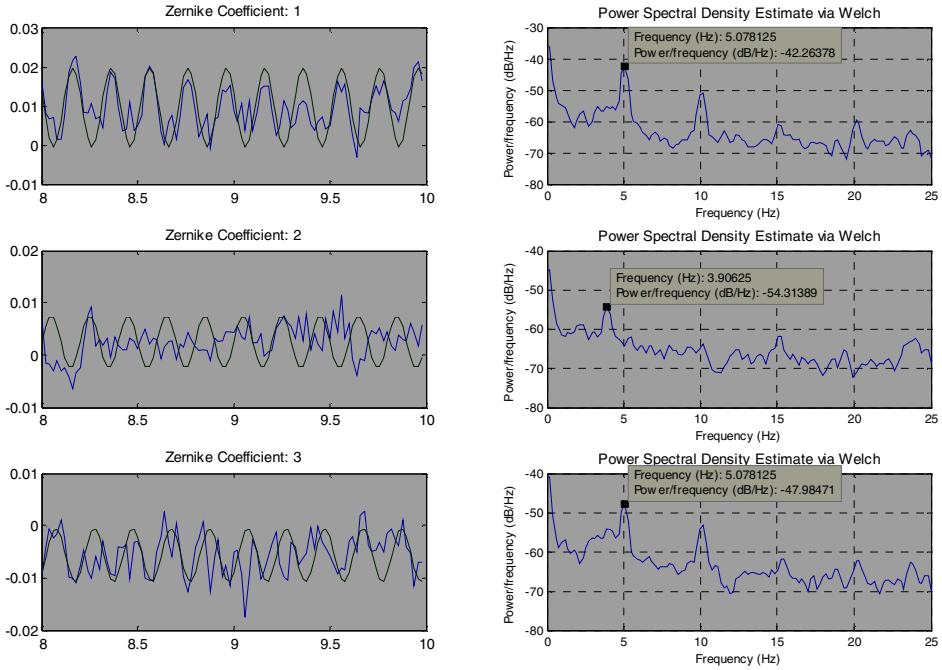

Figure 3.15 Frequency Response 5 Hz (Time Domain/Frequency Domain)

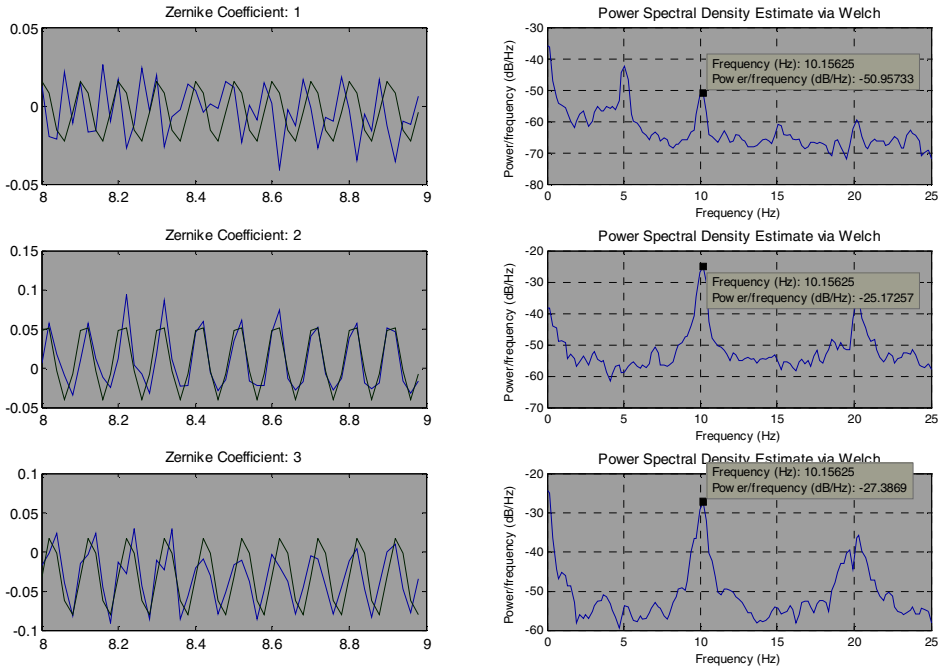

Figure 3.16 Frequency Response 10 Hz (Time Domain/Frequency Domain)

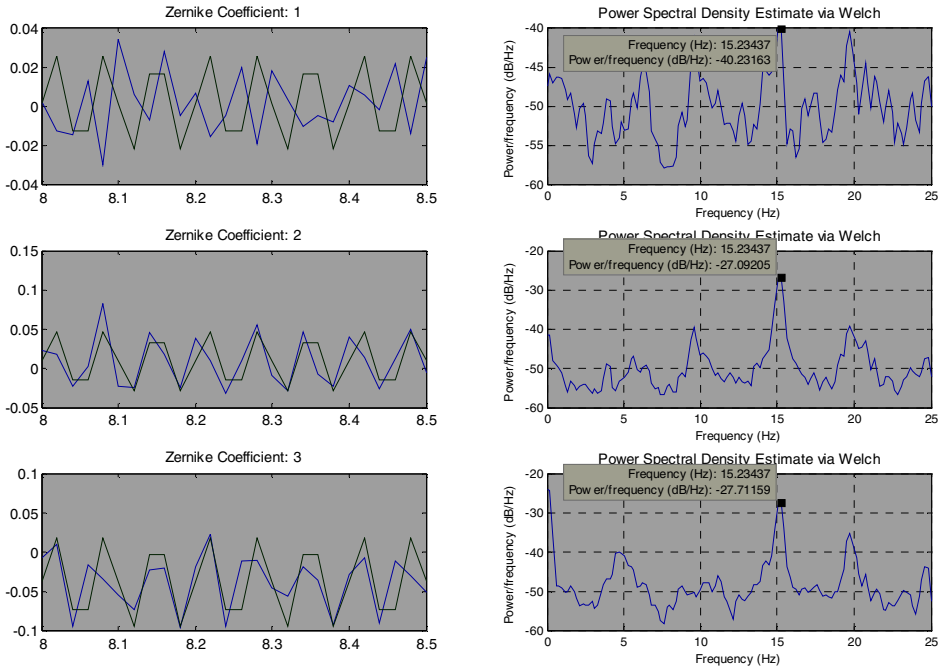

Figure 3.17 Frequency Response 15 Hz (Time Domain/Frequency Domain)

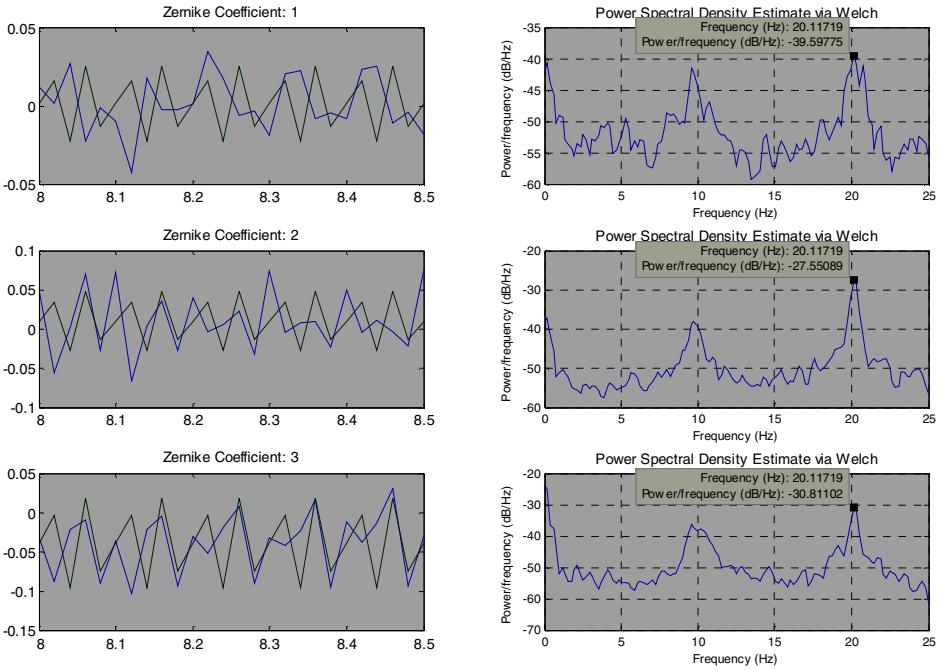

Figure 3.18 Frequency Response 20 Hz (Time Domain/Frequency Domain)

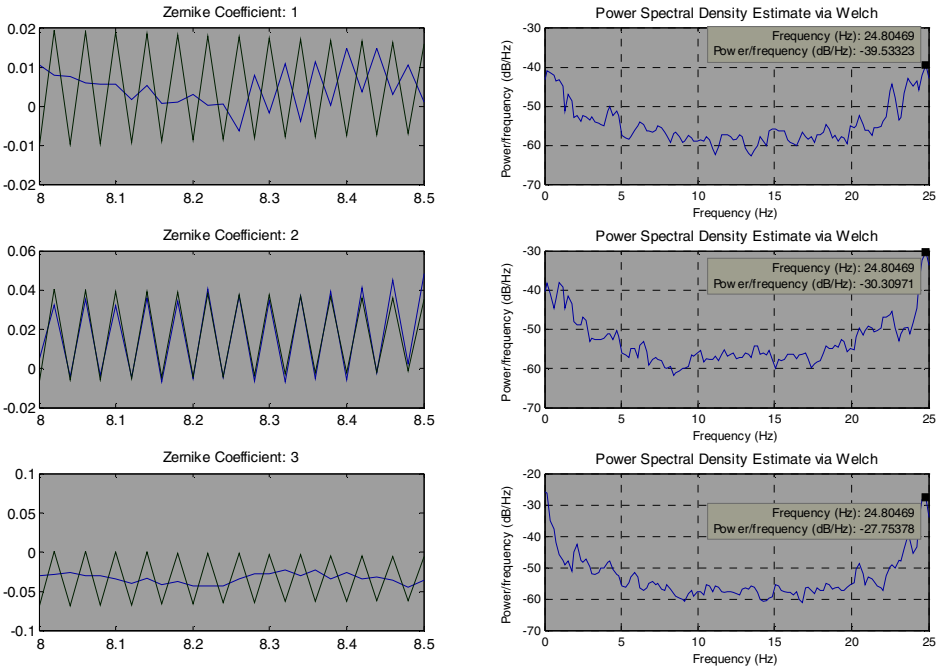

Figure 3.19 Frequency Response 25 Hz (Time Domain/Frequency Domain)

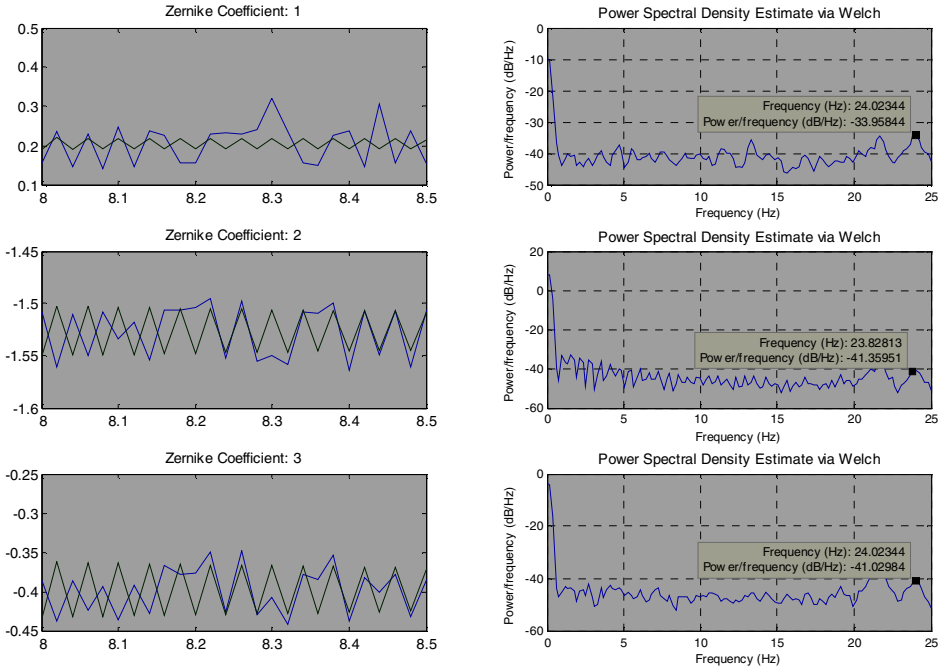

Figure 3.20 Frequency Response 27 Hz (Time Domain/Frequency Domain)

3.7 Summary

The combination of new fabrication techniques and a new data acquisition setup provide a more accurate test setup to evaluate any dynamic response on the membrane mirror. By more accurately controlling tilt and ensuring that all actuation patches are the same size and thickness, the new fabrication techniques remove significant sources of error in wavefront detection. Furthermore, the new data acquisition system allows dramatically faster sampling rates from preceding systems allowing an improved understanding of aliasing effects at higher frequencies that previously were lost. However, the throughput of the system is not fast enough to fully observe the dynamics of the membrane mirror.

IV. Results

4.1 Chapter Overview

This chapter will discuss the results of the work done to demonstrate dynamic closed loop control for an in-plane actuated deformable membrane mirror. It is important to note that due to damage to the newly fabricated mirror and time constraints, an older mirror constructed for the work done by Peterson [26] was used. Non-uniform reflectivity, 3 failed actuators and non-uniform charges on the 4 working actuators created extra noise on the mirror as well as contributing to a poor response.

4.2 Test Set-up

To demonstrate closed-loop dynamic control of our mirror requires four steps. The use of influence functions to control the shape of the mirror assumes that the deflections created by the actuation patches on the mirror are linear with respect to an increasing voltage. This assumption requires that the first step be to calculate the response of the mirror as the voltages are applied to each actuator. This data will be used to calculate the gain matrix that will be applied to the Zernike coefficients to convert them to voltages. The second step is to excite the actuation patches again and determine the level of deflection that the piezo voltages can create keeping the mirror within the range of the gain matrix calculated above. The third step is to apply the gain matrix to the streaming Zernike coefficients and develop a PID controller that will drive the closed loop error to zero. The fourth and last step is to disturb the mirror with a piezo stack, close the loop on the controller and drive the error and noise on the mirror to zero.

4.3 Gain Matrix

Previous researchers at AFIT have defined the Zernike IFS as the ratio of the change in magnitude of each Zernike coefficient per one volt applied to the actuators, Equation 4.1 [26]. Where H is a 7 x 7 matrix consisting of the Zernike IFS for all of the actuators, V is a diagonal matrix of scalar voltage steps, and Z is a matrix of Zernike which combines the Zernike coefficient vectors of the 7 actuators. The gain matrix K can then be calculated using H by using the assumption that the response of the mirror is linear, Equation 4.2.

$$H = V^{-1}Z \tag{4.1}$$

$$K = (H^T H)^{-1} H^T \tag{4.2}$$

To test the linearity of the mirror, a combination of two VIs were used to generate constant voltages from -600 to 600 with a 50 volt step in between data sets and then capture the associated Zernike coefficients (Appendix B.1 and B.2). A Matlab script found in Appendix A.1 then used Equations 4.1 and 4.2 above to calculate the influence functions for Actuators 1, 3, 4, and 5 using a pseudo inverse to calculate the gain matrix for the mirror as well as generated Figures 4.1 – 4.4 below which show all 7 Zernike coefficients plotted for Actuators 1, 3, 4, and 5 versus voltage. The pseudo inverse was used because the 7x7 matrix was padded with zeros which correspond to the influence functions for Actuators 2, 6, and 7. Analyzing the plots makes it clear that these responses are not linear with respect to an increase in voltage which can be attributed to the state of the mirror. However, the assumption that the mirror responds linearly to an increase in voltage is still maintained. This adds a significant source of error to the gain

matrix K and will impact surface deflections by the actuation patches but provides a close estimation to the voltage conversions for each Zernike coefficient.

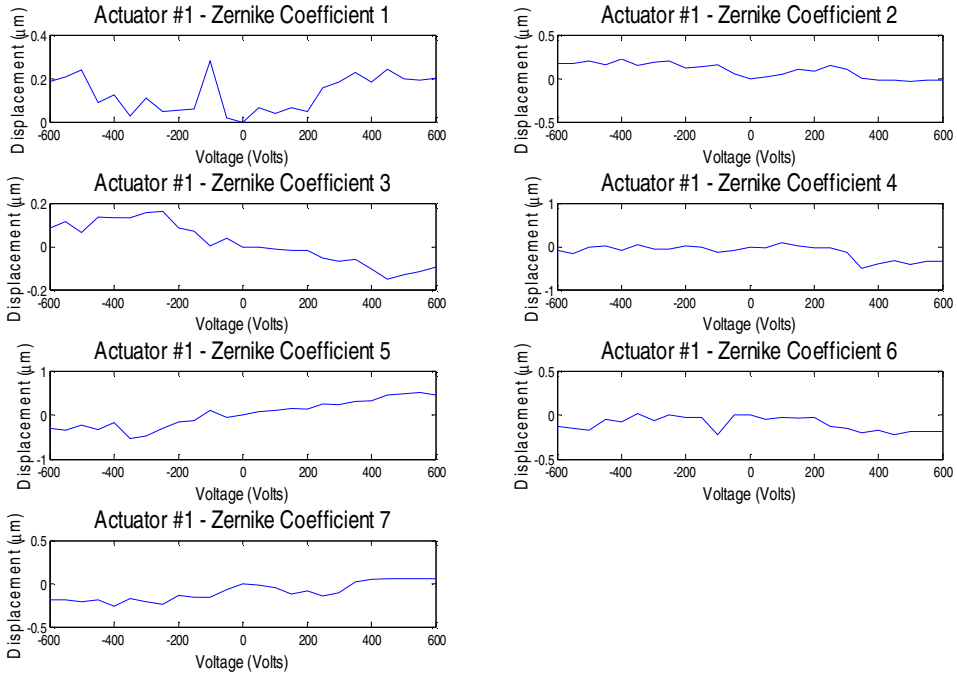

Figure 4.1 Response of Actuator 1

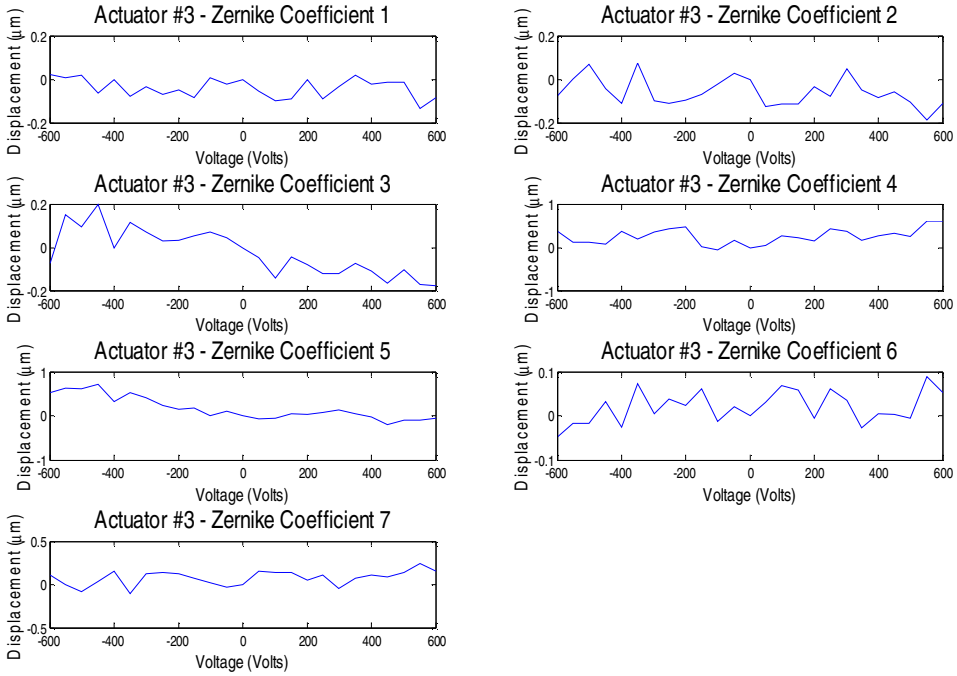

Figure 4.2 Response of Actuator 3

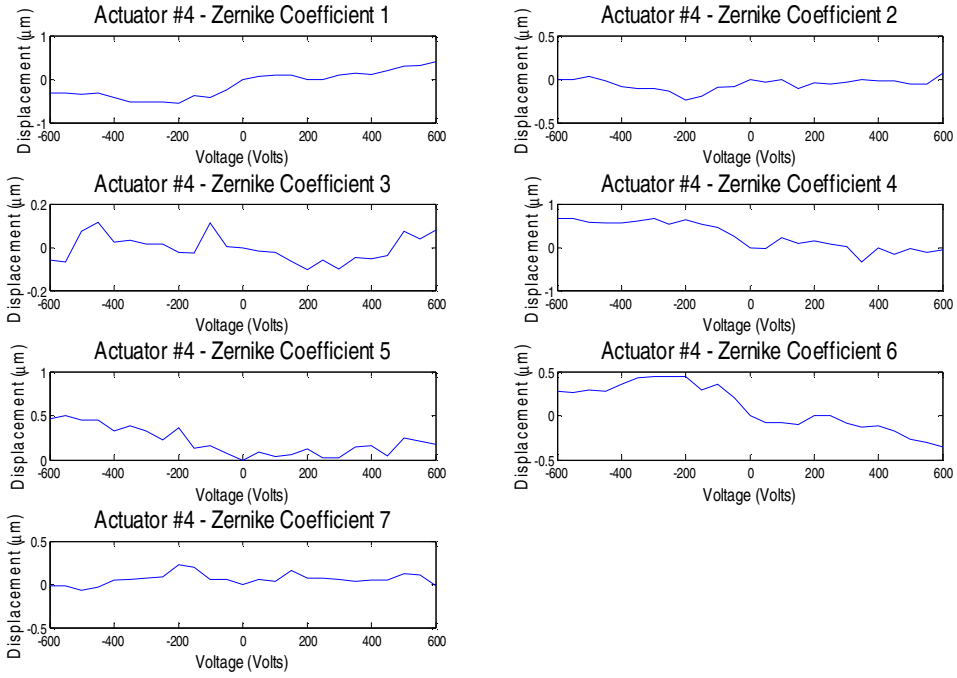

Figure 4.3 Response of Actuator 4

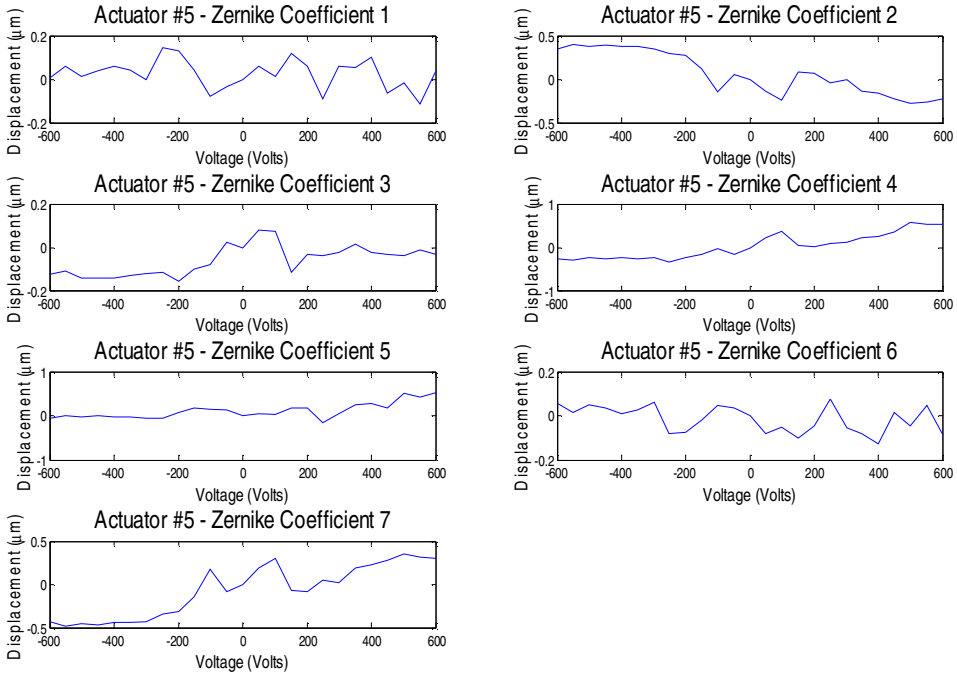

Figure 4.4 Response of Actuator 5

4.4 Actuator Limitations

To determine how much of an influence the piezo-electric actuators have over the Zernike coefficients for a given disturbance is determined by the linearity of the surface deflections caused by the actuators. Knowing how the system should respond based on the calculated K matrix, constant signals of -600 V, 0 V, and 600 V were applied to the mirror again and the Zernike coefficients were measured through Wavescope. The first step in the analysis is to subtract the 0 Volt data set from each data set. This zeros out each Zernike coefficient giving a common starting point for comparison. The influence of the actuators in the positive and negative direction is then calculated by comparing the -600 V data to the 0 V position and then the 600 V data to the 0 V position. This gives the total amount of influence each actuator has over each Zernike Coefficient, (Appendix A.4). Based on this analysis and Figure 4.5, it was determined that Actuator 3 and

Actuator 4 define how much influence that the actuators have over the seven desired Zernike coefficients. Moreover, the actuators have the ability in their current state of correct any errors which a surface deflection of ± 0.3 μm in the positive direction and negative directions.

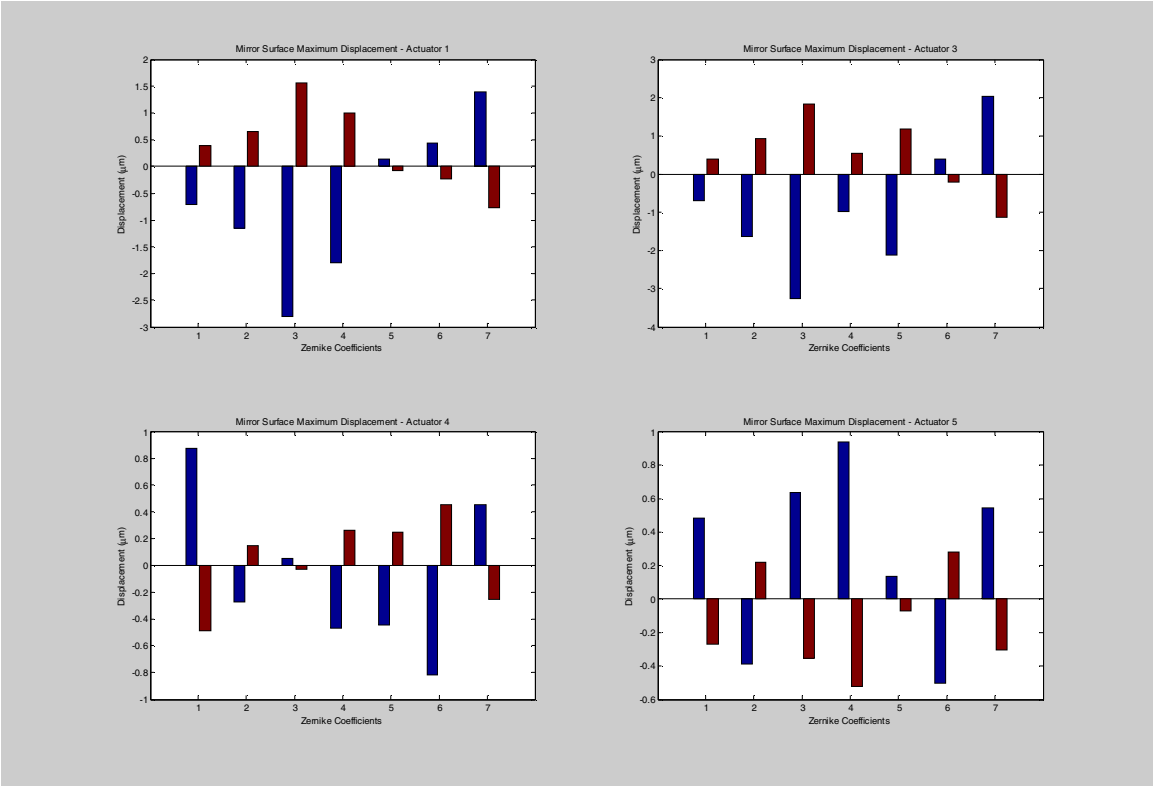

Figure 4.5 Actuator Influence over Zernike Coefficients

4.5 Controller

Now that K and the total the actuator influence have been calculated the final step in demonstrating dynamic control of an in-plane actuated membrane deformable mirror is to develop and implement a multiple single input multiple output (SIMO) controller and then test the controller by creating a dynamic disturbance that will translate to the mirror.

4.5.1 Piezo Stack Control

In order to simulate an external disturbance on the mirror, a piezo stack was placed under the aluminum frame of the mirror in the place of one of its three stabilizing posts (Figure 4.6). The piezo stack was purchased from Piezo Systems, Inc. and is capable of 14.5 µm of deflection and is rated for only positive voltages with a maximum of 100 Volts DC. To put a sinusoidal signal on the piezo stack a 40 volt bias was placed on it allowing the piezo stack to expand and contract. Previous work completed at AFIT characterized the piezo stack and for a ½ Hz a 10 volt amplitude sinusoid will give approximately 0.1 µm of deflection [26]. To achieve 0.3 µm of deflection a 30 volt sine wave was generated by a VI created for that purpose (Appendix B.5).

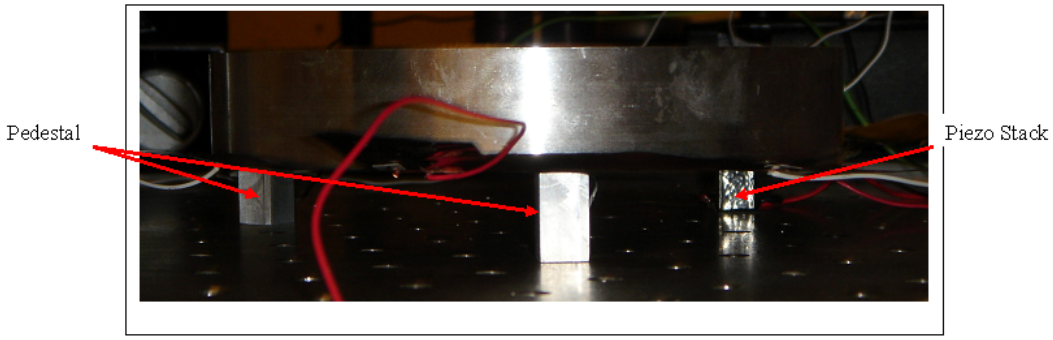

Figure 4.6 Piezo Stack Setup

4.5.2 Control Design and Implementation

The goal of the controller in the current configuration is to drive the mirror surface to a flat position. Defining the flat position again as the Wavescope measurement of the surface of the mirror with a zero voltage applied to it; the average of each Zernike coefficient is then calculated.

The designed single input multiple output (SIMO) controller implements Proportional-Integral-Derivative (PID) control in a feedback loop (Equation 4.3).

$$Control = K_p e(t) + K_i \int_0^t e(\tau)d\tau + K_d \frac{de}{dt} \quad \textbf{(4.3)}$$

The gain matrix K, is applied to the incoming Zernike coefficients of the disturbed mirror the PID controller subtracts these values from the Zernike coefficients corresponding to a flat mirror position and generates voltages that are applied to the actuation patches to drive the error between the flat and disturbed mirror to zero (Figure 4.7).

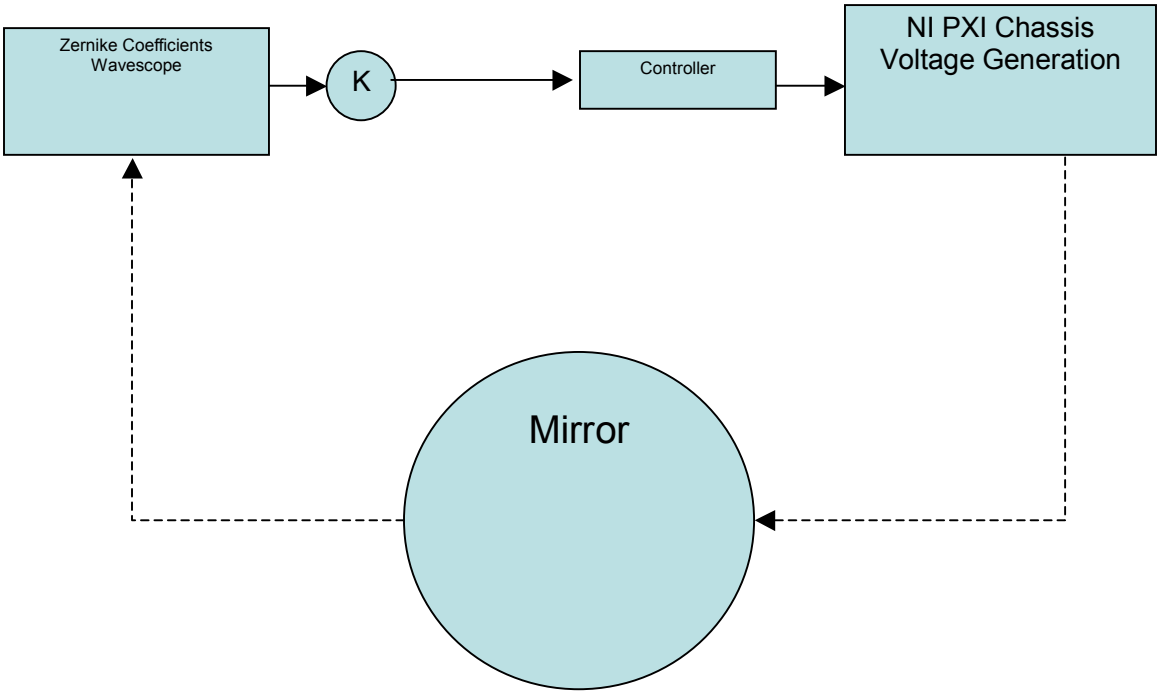

Figure 4.7 Simplified Block Diagram of Feedback Controller

The Zernike coefficients for the flat mirror were measured in Wavescope and then hard wired into the PID controller, Table 4.1. Furthermore, the output Voltage was limited to ±600 volts to prevent over stressing the PVDF. Once this was complete, a 0.5 Hz disturbance was placed on the mirror and the proportional gain (K_p), integral gain (K_i) and derivative gain (K_d) were set to 1. Then the loop was closed on the controller. K_p, K_i and K_d were then varied until the error was driven down to approximately zero. It is important to note the trade offs for changing each gain. The resulting gains are in Table

4.2. The large sources of error due to the linearization assumption can explain why the K_i terms are all zero.

Table 4.1 Zernike Coefficients for a Flat Mirror

Zernike Coefficient	Position
1	2.9
2	1.87
3	-3.2
4	2.25
5	2.89
6	-2.5
7	-0.28

Table 4.2 Proportional, Integral and Derivative Control Values

	Act 1	Act 2	Act 3	Act 4	Act 5	Act 6	Act 7
Kp	-0.084	0	-0.084	-0.084	-0.084	0	0
Ki	0	0	0	0	0	0	0
Kd	-1	0	-10	-7	-6.007	0	0

Once the PID gains were set based on the 0.5 Hz disturbance three more test cases were done with a 1 Hz, 5 Hz and 10 Hz disturbance on the mirror holding the gains constant to determine how well the controller could dampen out disturbances at higher frequencies.

4.5.3 Results

Working with 4 out of 7 actuators coupled with the deteriorated state of the membrane mirror coupled with a disturbance that exceeded actuator capabilities prevented the controller from driving the error in any of the seven Zernike coefficients to zero. Figure 4.9-4.12 below show the disturbance response next to the controller response to that disturbance. The disturbance was lost in the mirror noise at 0.3 μm so the disturbance was increased to 0.45 μm. At that magnitude the actuators began to drive the error in the system to the set point, 1.8 μm but never eliminate the error associated with a disturbance at 0.5 Hz in the Y tilt direction. These results are supported by knowing the orientation of the mirror and how Wavescope defined the x-y plane of the mirror (Figure 4.8). Knowing this orientation helps to support the plots because three active actuation patches were oriented to create or remove tilts in the y direction as opposed to only 2 active actuation patches in the x direction. Moreover, as the frequency of the disturbance was increased from 0.5 Hz to 10 Hz the ability to track the disturbance is lost completely.

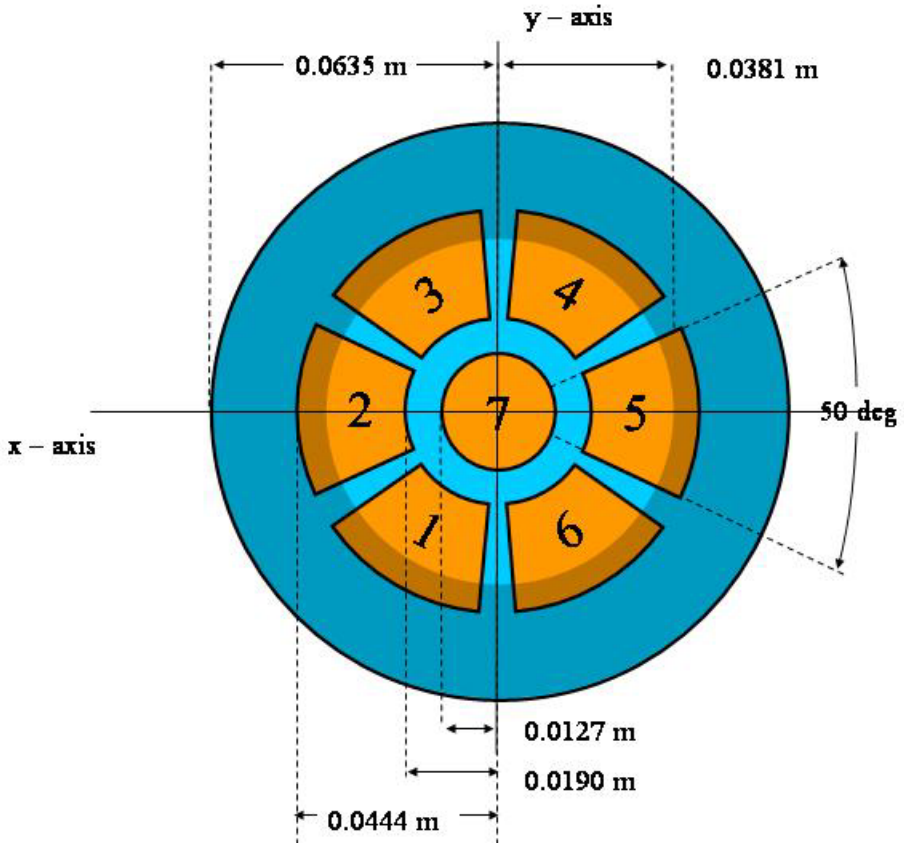

Figure 4.8 Mirror Orientation in the X – Y Plane in Wavescope

These results were expected due to the condition of the current mirror. The non-linear nature of the mirror and the corresponding error in the controller prevents the mirror from driving the disturbance to zero. Moreover, the noise associated with these non-linearities also creates a situation where the magnitude of the disturbance necessary to be measured in Wavescope is greater than the capabilities of the actuation patches.

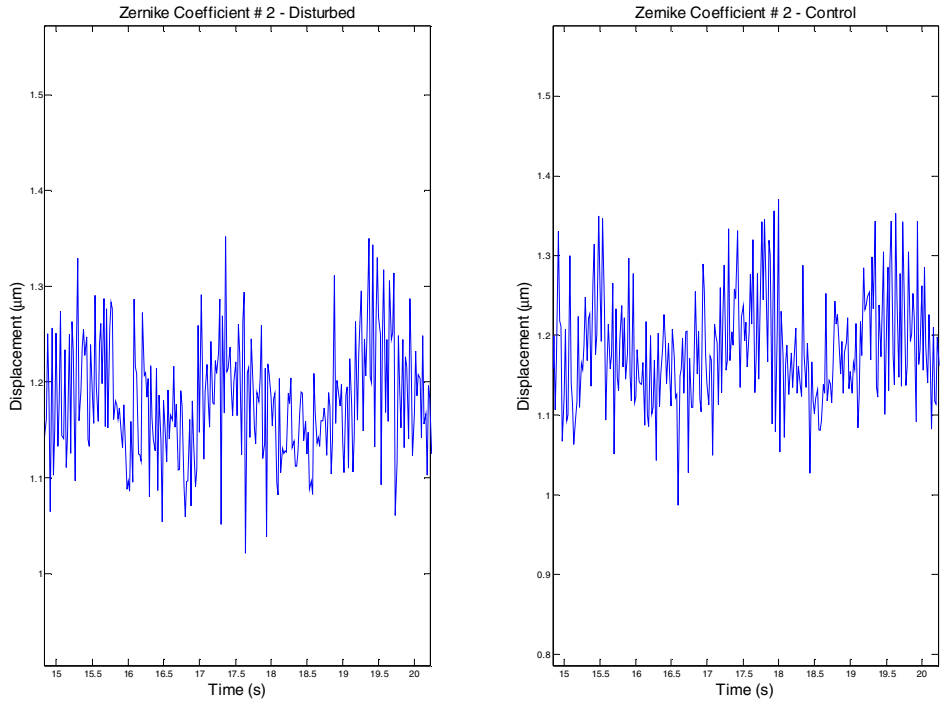

Figure 4.9 0.5 Hz Sinusoidal Disturbance (Uncontrolled /Controlled)

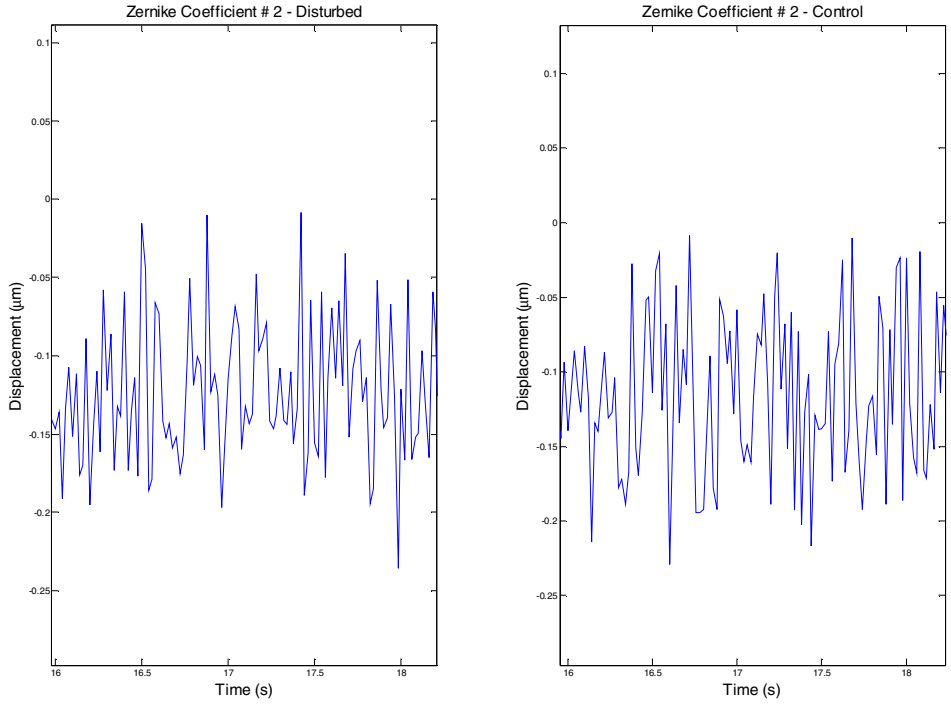

Figure 4.10 Residual Controller Errors to a 5 Hz Sinusoidal Disturbance

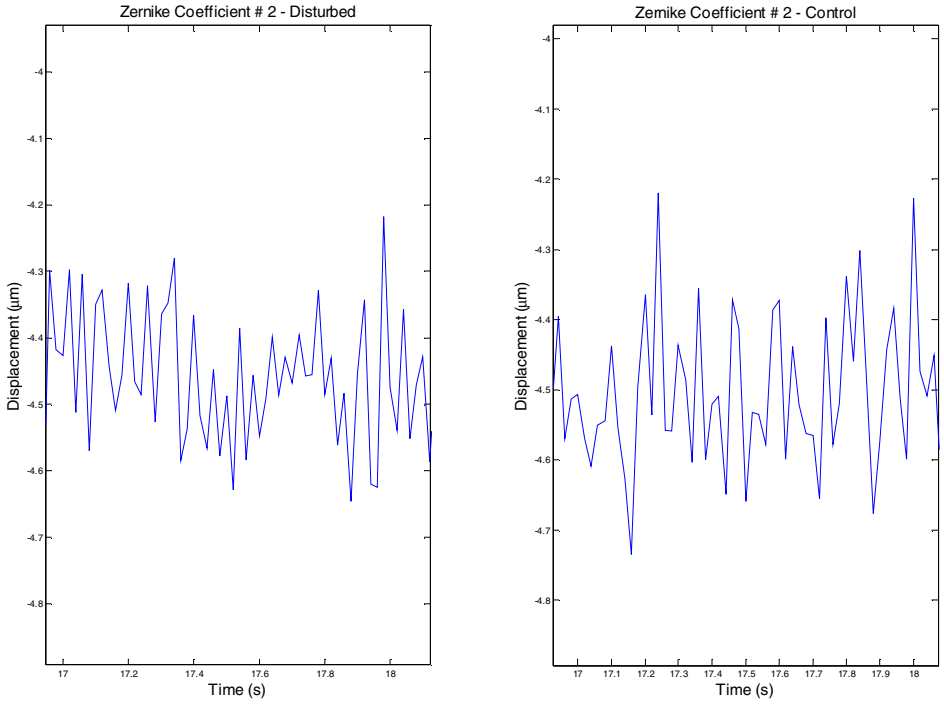

Figure 4.11 Residual Controller Errors to a 10 Hz Sinusoidal Disturbance

4.6 Summary

This chapter begins by discussing the test set-up created to demonstrate dynamic closed-loop control of an in-plane actuated membrane mirror. It then describes how the influence functions of the mirror and gain matrix are calculated based on the mirror responding linearly to voltage increases, and the fact that the mirror responds in a non-linear fashion. Next it discusses the calculations made to determine the amount of control the actuators will have on changing the Zernike coefficients. This is followed by details on how the actual controller was developed before finally demonstrating that the implemented control algorithm could not eliminate the error associated with any disturbance applied.

V. Conclusions and Recommendations

5.1 Overview

This research set three objectives to demonstrate dynamic closed-loop control of an in-plane actuated deformable membrane mirror. The first objective was to setup and validate a new data acquisition system. The second was to implement new fabrication techniques based on recommendations from previous work done at AFIT. Finally the third was to demonstrate dynamic closed-loop control of an in-plane actuated membrane mirror.

5.2 Conclusions

The switch from the D-Space setup to the NI PXI Chassis setup was a complete success. An interface was successfully created between Chassis and the Wavescope sensor. Based on the Zernike coeffiecients calculated by Wavescope the Chassis calculates voltages that are amplified and applied to an in-plane actuated membrane mirror. More importantly, frequency and time plots of an applied sinusoidal wave at different frequencies validated that the throughput of the system was increased from 2.5 Hz to 50 Hz. However, this seems to be as fast as Labview can parse the data in the ASCII format.

The modification of fabrication techniques for the creation of an in-plane actuated membrane mirror met with limited success. First the aluminum ring design was modified to allow for better mounting and the ability to remove tilts on the mirror. This proved to be an important step because the old method of mounting the mirror used three optical screws with electrical tape to suspend the ring. Overtime the tape began to wear down which caused the electric potential to jump to ground leading to an electrical fire that

burned through the PVDF ruining the mirror. Second, the silver paint used for electrodes was evaporated onto the etched PVDF using an aluminum template. This allowed for a more uniform capacitance across the actuator patches because the amount of silver paint could be better controlled and all of the actuation patches were uniform in size. The excess PVDF was removed from the mirror and the electrodes were shortened coming to an end at the outer perimeter of the aluminum ring. This was successful in preventing cracking in the electrode due to bending but failed because the first time 600 Volts was placed on one of the electrodes, the minimal distance between the electrode and the aluminum ring caused by cutting away all of the excess PVDF allowed the electric potential to jump to ground again leading to an electrical fire that burned through the PVDF ruining the new mirror. As a result, the fabrication process was modified again to etch the PVDF prior to bonding it to the aluminum ring and to leave approximately 1" of PVDF around the outside of the ring to prevent any rounding issues that could have caused the localized grounding.

The demonstration of dynamic closed-loop control of an in-plane actuated membrane mirror was not successful. The use of an older mirror that had only 4 functional actuation patches, non-uniform reflectivity, and non-uniform conductivity created influence functions for the 4 actuators were did not respond in a linear fashion and created an enormous source of noise. The assumption was still made that the influence functions were linear in calculating the gain matrix, K which creates another source of error. While the controller begins to drive towards the set point at low frequencies in the Y-tilt direction it does not reach its goal because the disturbance on the

mirror is greater then the capabilities of the actuation patches. It is also unclear if the controller works to damp higher frequency disturbances that are applied to the mirror.

5.3 Recommendations for Future Research

The six areas that can be improved upon for future research endeavors are the fabrication process, the data acquisition setup and controller development.

First, the current fabrications techniques create too much variation from mirror to mirror which means that each mirror will need to be individually characterized and a unique controller developed for each mirror. Furthermore, exploring methods to eliminate the non-linear properties from the mirror surface so that the surface responds linearly to voltage increases will provide a more accurate gain matrix and all for more surface control.

Second, the data acquisition needs to be improved so that the throughput of the system is greater then 50Hz. One avenue to explore would be to identify the pattern to the Wavescope binary data output. The theoretical data rate that the Wavescope sensor can output in the binary format is 34 Hz for all 42 Zernike coefficients and 198 Hz for 7 Zernike coefficients. Coupled with increasing the speed of the Wavescope output is to decrease the time necessary to parse the data in Labview. The alternative to this is to investigate the possibility of improving the read out electronics of the sensor to increase the data rate of the Wavescope output.

The third area that needs to be explored is a trade off analysis of the number of Zernike coefficients necessary to completely control the surface of the mirror. The decision was made to use only the first 7 Zernike coefficients for this research to increase

the system throughput but identifying the optimal number of Zernike coefficients should be identified.

While this research demonstrates dynamic closed-loop control of an in-plane actuated membrane mirror assumptions were made about the mirror that was known to be false. By assuming the mirror responded linearly introduced a slew of errors that prevented the controller from working correctly. The fourth area to explore is to fabricate a new mirror using the updated fabrication techniques, and reproduce the work done here in. By using a new mirror that responds linearly to increasing voltages will aid in calculating influence functions that more accurately model the characteristics of the actuation patches and should be able to drive all of the residual error to zero.

The fifth area of improvement would be to implement the PID controller and in lieu of using a guess and check method utilize an optimization search code such as fmincon in Matlab to optimize K_p, K_i, and K_d for the controller. Furthermore, by implementing a gain schedule that takes into account the increasing frequency of external disturbances could possibly allow for greater control over a larger frequency spectrum.

Appendix A. Matlab Code

A.1 Linearization Code

```
clear all;clc;
zmean = zeros(7,42);
for n = 1:4
    ZStotal=zeros(42,25);
    x = [-600:50:600];
    zs = zeros(25,42,500);
    if n == 1
        cd('I:\Thesis\Gabriele\Final Data\Final Tests\Linear
Data\Actuator 1')
    elseif n == 2
        cd('I:\Thesis\Gabriele\Final Data\Final Tests\Linear
Data\Actuator 3')
    elseif n == 3
        cd('I:\Thesis\Gabriele\Final Data\Final Tests\Linear
Data\Actuator 4')
    elseif n == 4
        cd('I:\Thesis\Gabriele\Final Data\Final Tests\Linear
Data\Actuator 5')
    end
    zss = zeros(42,25);
    zsss = zeros(42,24);
    static = zeros(42,500);
    FileName = ['Data00.txt';'Data01.txt';'Data02.txt';'Data03.txt';...

'Data04.txt';'Data05.txt';'Data06.txt';'Data07.txt';'Data08.txt';...

'Data09.txt';'Data10.txt';'Data11.txt';'Data12.txt';'Data13.txt';...

'Data14.txt';'Data15.txt';'Data16.txt';'Data17.txt';'Data18.txt';...

'Data19.txt';'Data20.txt';'Data21.txt';'Data22.txt';'Data23.txt';...
        'Data24.txt'];
    StaticFile=load('Data12.txt');
    t = reshape(StaticFile,7,500);
    static(1:7,:) = t;
    for ii = 1:25
        P(ii,:) = load(FileName(ii,:));
    end
    Q=reshape(P,25,7,500);

    zs(:,1:7,:) = Q;

    for k = 1:42
        for ii = 1:25
            zss(n,k,ii) = mean(zs(ii,k,:))-mean(static(k,:));
            if ii ~= 1
                zsss(k,ii-1)=zss(n,k,ii)-zss(n,k,ii-1);
            end
        end
        if n == 1
            zmean(1,k)=mean(zsss(k,:));
```

```
            zstd(1,k)=std(zsss(k,:));
        elseif n == 2
            zmean(3,k)=mean(zsss(k,:));
            zstd(3,k)=std(zsss(k,:));
        elseif n == 3
            zmean(4,k)=mean(zsss(k,:));
            zstd(4,k)=std(zsss(k,:));
        elseif n == 4
            zmean(5,k)=mean(zsss(k,:));
            zstd(5,k)=std(zsss(k,:));
        end

    end

    figure;
    for l = 1:7
        subplot(4,2,l)
        T(:,:) = zss(n,l,:);
        plot(x,T)
        if n == 1
            title(['Actuator #',num2str(n),' - Zernike Coefficient
',num2str(l)]);
        else
            title(['Actuator #',num2str(n+1),' - Zernike Coefficient
',num2str(l)]);
        end
        xlabel('Time (s)')
        ylabel('Displacement ({\mu}m)')
    end
end

A = (zmean)';
A = A./50;
K = pinv(A'*A)*A';
K=K./200;
```

A.2 Parsing Zernike Coeffiecent Output

```
%-------------------------------------------------------------------------
function [z] = PD42Zern(Dir,Filename);
cd(Dir)
A = zeros(210000,1);
A=load(Filename);

for jj = 1:42
    for ii = 1:5000
        Tempz(jj,ii)=A(ii*42-(42-jj));
    end
end
for hh = 1:42
    count = 1;
    for ii = 1:25
        for jj = 1:200
            z(hh,ii,jj)=Tempz(hh,count);
            count = count+1;
        end
    end
end
```

A.3 Rate Test Code

```
%-------------------------------------------------------------------------
% Actuator: Rate Test
clear all; close all; clc;
x = 0.02*[1:800];
dir = ['C:\Documents and Settings\Gabriele\Final Tests\RateTest']
cd(dir)
A=['Flat00Hz.txt';'Data01Hz.txt';'Data05Hz.txt';'Data10Hz.txt';'Data15H
z.txt';...
    'Data20Hz.txt';'Data25Hz.txt'];
B =
['Flat00Hz1.txt';'Data01Hz1.txt';'Data05Hz1.txt';'Data10Hz1.txt';...
    'Data15Hz1.txt';'Data20Hz1.txt';'Data25Hz1.txt'];
for ii = 1:7
    Data(ii,:) = load(A(ii,:));
    Data1(ii,:) = load(B(ii,:));
end
Flat = reshape(Data(1,:),7,800);
TempData = Data(2:7,:);
zi = reshape(TempData,6,7,800);
Flat1 = reshape(Data1(1,:),7,800);
TempData1 = Data1(2:7,:);
zi1 = reshape(TempData1,6,7,800);
for ii = 1:7
    mFlat(ii) = mean(Flat(ii,:));
    mFlat1(ii) = mean(Flat1(ii,:));
    sig01Hz(ii,:) = zi(1,ii,:)-mFlat(ii);
    sig05Hz(ii,:) = zi(2,ii,:)-mFlat(ii);
    sig10Hz(ii,:) = zi(3,ii,:)-mFlat(ii);
    sig15Hz(ii,:) = zi(4,ii,:)-mFlat(ii);
    sig20Hz(ii,:) = zi(5,ii,:)-mFlat(ii);
```

```
    sig25Hz(ii,:) = zi(6,ii,:)-mFlat(ii);
    sig01Hz1(ii,:) = zi1(1,ii,:)-mFlat1(ii);
    sig05Hz1(ii,:) = zi1(2,ii,:)-mFlat1(ii);
    sig10Hz1(ii,:) = zi1(3,ii,:)-mFlat1(ii);
    sig15Hz1(ii,:) = zi1(4,ii,:)-mFlat1(ii);
    sig20Hz1(ii,:) = zi1(5,ii,:)-mFlat1(ii);
    sig25Hz1(ii,:) = zi1(6,ii,:)-mFlat1(ii);
end
%-------------------------------------------------------------------------
%## 1 Hz ##
figure;subplot(3,2,1);
plot(x(400:599),sig01Hz(1,400:599),x(400:599),0.025*sin(2*pi*x(400:599)
-8.85)+0.001)
title('Zernike Coefficient: 1');
subplot(3,2,2);pwelch(sig01Hz(1,:),[],[],[],50);
subplot(3,2,3);
plot(x(400:599),sig01Hz(2,400:599),x(400:599),0.025*sin(2*pi*x(400:599)
+.95))
title('Zernike Coefficient: 2');
subplot(3,2,4);pwelch(sig01Hz(2,:),[],[],[],50);
subplot(3,2,5);
plot(x(400:599),sig01Hz(3,400:599),x(400:599),0.075*sin(2*pi*x(400:599)
+0.75)+mean(sig01Hz(3,400:599)))
title('Zernike Coefficient: 3');
subplot(3,2,6);pwelch(sig01Hz(3,:),[],[],[],50);
%-------------------------------------------------------------------------
%## 5 Hz ##
figure;subplot(3,2,1);
plot(x(400:499),sig05Hz(1,400:499),x(400:499),0.01*sin(10*pi*x(400:499)
-3.5)+mean(sig05Hz(1,400:499)))
title('Zernike Coefficient: 1');
subplot(3,2,2);pwelch(sig05Hz(1,:),[],[],[],50);
subplot(3,2,3);
plot(x(400:499),sig05Hz(2,400:499),x(400:499),0.005*sin(10*pi*x(400:499
))+mean(sig05Hz(2,400:499)))
title('Zernike Coefficient: 2');
subplot(3,2,4);pwelch(sig05Hz(2,:),[],[],[],50);
subplot(3,2,5);
plot(x(400:499),sig05Hz(3,400:499),x(400:499),0.0051*sin(10*pi*x(400:49
9)-.75)+mean(sig05Hz(3,400:499)))
title('Zernike Coefficient: 3');
subplot(3,2,6);pwelch(sig05Hz(3,:),[],[],[],50);
%-------------------------------------------------------------------------
%## 10 Hz ##
figure;subplot(3,2,1);
plot(x(400:449),sig10Hz(1,400:449),x(400:449),0.02*sin(20*pi*x(400:449)
+1.25)+mean(sig10Hz(1,400:449)))
title('Zernike Coefficient: 1');
subplot(3,2,2);pwelch(sig05Hz(1,:),[],[],[],50);
subplot(3,2,3);plot(x(400:449),sig10Hz(2,400:449),x(400:449),0.05*sin(2
0*pi*x(400:449)+.90)+mean(sig10Hz(2,400:449)))
title('Zernike Coefficient: 2');
subplot(3,2,4);pwelch(sig10Hz(2,:),[],[],[],50);
subplot(3,2,5);plot(x(400:449),sig10Hz(3,400:449),x(400:449),0.051*sin(
20*pi*x(400:449))+mean(sig10Hz(3,400:449)))
title('Zernike Coefficient: 3');
subplot(3,2,6);pwelch(sig10Hz(3,:),[],[],[],50);
```

```
%-------------------------------------------------------------------------
%## 15 Hz ##
figure;subplot(3,2,1);
plot(x(400:425),sig15Hz(1,400:425),x(400:425),0.025*sin(30*pi*x(400:425
))+mean(sig15Hz(1,400:425)))
title('Zernike Coefficient: 1');
subplot(3,2,2);pwelch(sig15Hz(1,:),[],[],[],50);
subplot(3,2,3);
plot(x(400:425),sig15Hz(2,400:425),x(400:425),0.04*sin(30*pi*x(400:425)
)+mean(sig15Hz(2,400:425)))
title('Zernike Coefficient: 2');
subplot(3,2,4);pwelch(sig15Hz(2,:),[],[],[],50);
subplot(3,2,5);
plot(x(400:425),sig15Hz(3,400:425),x(400:425),0.06*sin(30*pi*x(400:425)
)+mean(sig15Hz(3,400:425)))
title('Zernike Coefficient: 3');
subplot(3,2,6);pwelch(sig15Hz(3,:),[],[],[],50);
%-------------------------------------------------------------------------
%## 20 Hz ##
figure;subplot(3,2,1);
plot(x(400:425),sig20Hz(1,400:425),x(400:425),0.025*sin(40*pi*x(400:425
))+mean(sig20Hz(1,400:425)))
title('Zernike Coefficient: 1');
subplot(3,2,2);pwelch(sig20Hz(1,:),[],[],[],50);
subplot(3,2,3);
plot(x(400:425),sig20Hz(2,400:425),x(400:425),0.04*sin(40*pi*x(400:425)
)+mean(sig20Hz(2,400:425)))
title('Zernike Coefficient: 2');
subplot(3,2,4);pwelch(sig20Hz(2,:),[],[],[],50);
subplot(3,2,5);
plot(x(400:425),sig20Hz(3,400:425),x(400:425),0.06*sin(40*pi*x(400:425)
)+mean(sig20Hz(3,400:425)))
title('Zernike Coefficient: 3');
subplot(3,2,6);pwelch(sig20Hz(3,:),[],[],[],50);
%-------------------------------------------------------------------------
%## 25 Hz ##
figure;subplot(3,2,1);
plot(x(400:425),sig25Hz(1,400:425),x(400:425),0.025*sin(50*pi*x(400:425
))+mean(sig25Hz(1,400:425)))
title('Zernike Coefficient: 1');
subplot(3,2,2);pwelch(sig25Hz(1,:),[],[],[],50);
subplot(3,2,3);
plot(x(400:425),sig25Hz(2,400:425),x(400:425),0.04*sin(50*pi*x(400:425)
)+mean(sig25Hz(2,400:425)))
title('Zernike Coefficient: 2');
subplot(3,2,4);pwelch(sig25Hz(2,:),[],[],[],50);
subplot(3,2,5);
plot(x(400:425),sig25Hz(3,400:425),x(400:425),0.06*sin(50*pi*x(400:425)
)+mean(sig25Hz(3,400:425)))
title('Zernike Coefficient: 3');
subplot(3,2,6);pwelch(sig25Hz(3,:),[],[],[],50);
```

A.4 Max Change to Coefficients

```
clear all;close all;clc;
cd('I:\Thesis\Gabriele\Final Data\Final Tests\Control');
FlatData = load('Flat00.txt');
Flat = reshape(FlatData,42,4000);
plot(Flat(1,:))
for ii = 1:7
    mF(ii) = mean(Flat(ii,:));
end

cd('I:\Thesis\Gabriele\Final Data\Final Tests\Linear Data\Actuator 3')
D1 = load('LData00.txt');
cd('I:\Thesis\Gabriele\Final Data\Final Tests\Linear Data');
load('Kmat.mat')
cd('I:\Thesis\Gabriele\Final Data\Final Tests\Control');
D2 = load('LData02.txt');
B1 = load('LData01.txt');

Dat1 = reshape(D1,42,1000);
Dat2 = reshape(D2,42,1000);
V = reshape(B1,42,1000);

for ii = 1:7
    Dt1(ii,:) = Dat1(ii,:)-mF(ii);
    Dt2(ii,:) = Dat2(ii,:)-mF(ii);
    B(ii,:) = V(ii,:)-mF(ii);



    Tcalc = mean(Dt1(ii,:)-B(ii,:))*K;
    Tcalc2 = mean(Dt2(ii,:)-B(ii,:))*K;
end
range = [Tcalc;Tcalc2];
range1(1:2,:) = [Tcalc(1,1:7); Tcalc2(1,1:7)];
range3(1:2,:) = [Tcalc(3,1:7); Tcalc2(3,1:7)];
range4(1:2,:) = [Tcalc(4,1:7); Tcalc2(4,1:7)];
range5(1:2,:) = [Tcalc(5,1:7); Tcalc2(5,1:7)];
subplot(2,2,1)
bar (range1', 'DisplayName', 'range1(1:2,1)', 'YDataSource',
'range1(1:2,1)'); figure(gcf)
title('Mirror Surface Maximum Displacement - Actuator 3')
xlabel('Zernike Coefficients')
ylabel('Displacement ({\mu}m)')
subplot(2,2,2)
bar (range3', 'DisplayName', 'range1(1:2,1)', 'YDataSource',
'range1(1:2,1)'); figure(gcf)
title('Mirror Surface Maximum Displacement - Actuator 3')
xlabel('Zernike Coefficients')
ylabel('Displacement ({\mu}m)')
subplot(2,2,3)
bar (range4', 'DisplayName', 'range1(1:2,1)', 'YDataSource',
'range1(1:2,1)'); figure(gcf)
title('Mirror Surface Maximum Displacement - Actuator 3')
xlabel('Zernike Coefficients')
ylabel('Displacement ({\mu}m)')
```

```
subplot(2,2,4)
bar (range5', 'DisplayName', 'range1(1:2,1)', 'YDataSource',
'range1(1:2,1)'); figure(gcf)
title('Mirror Surface Maximum Displacement - Actuator 3')
xlabel('Zernike Coefficients')
ylabel('Displacement ({\mu}m)')
```

Appendix B Labview VIs

B.1 Zernike Out VI

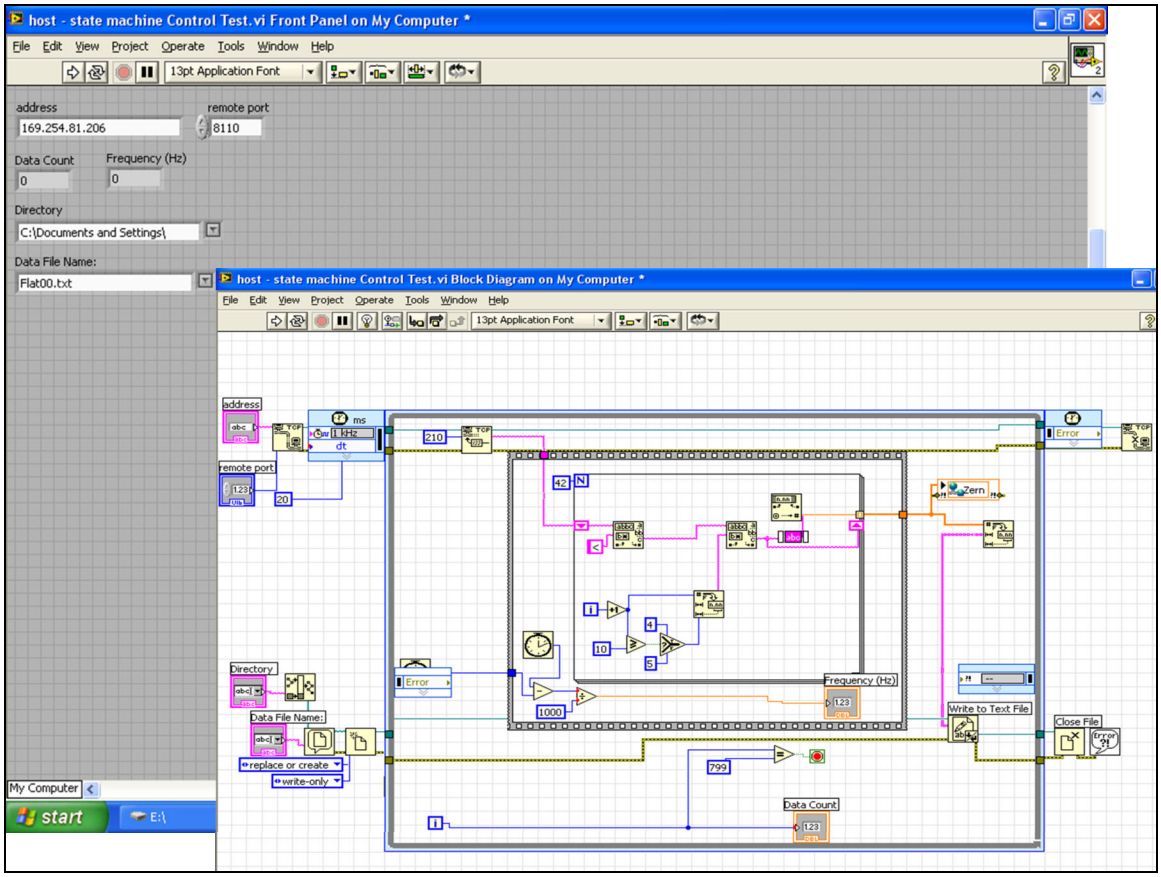

B.2 Rate Test Voltage Generation VI

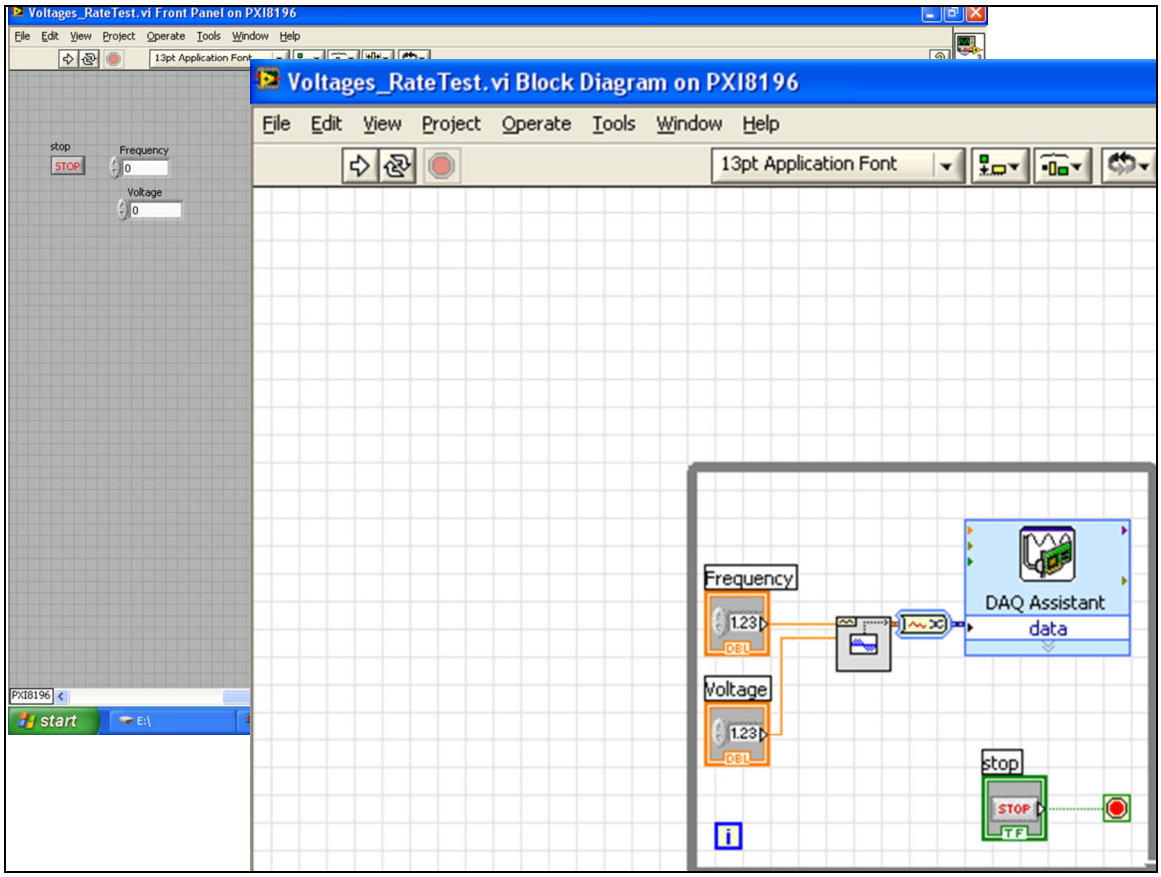

B.3 Linearity Test Voltage Generation VI

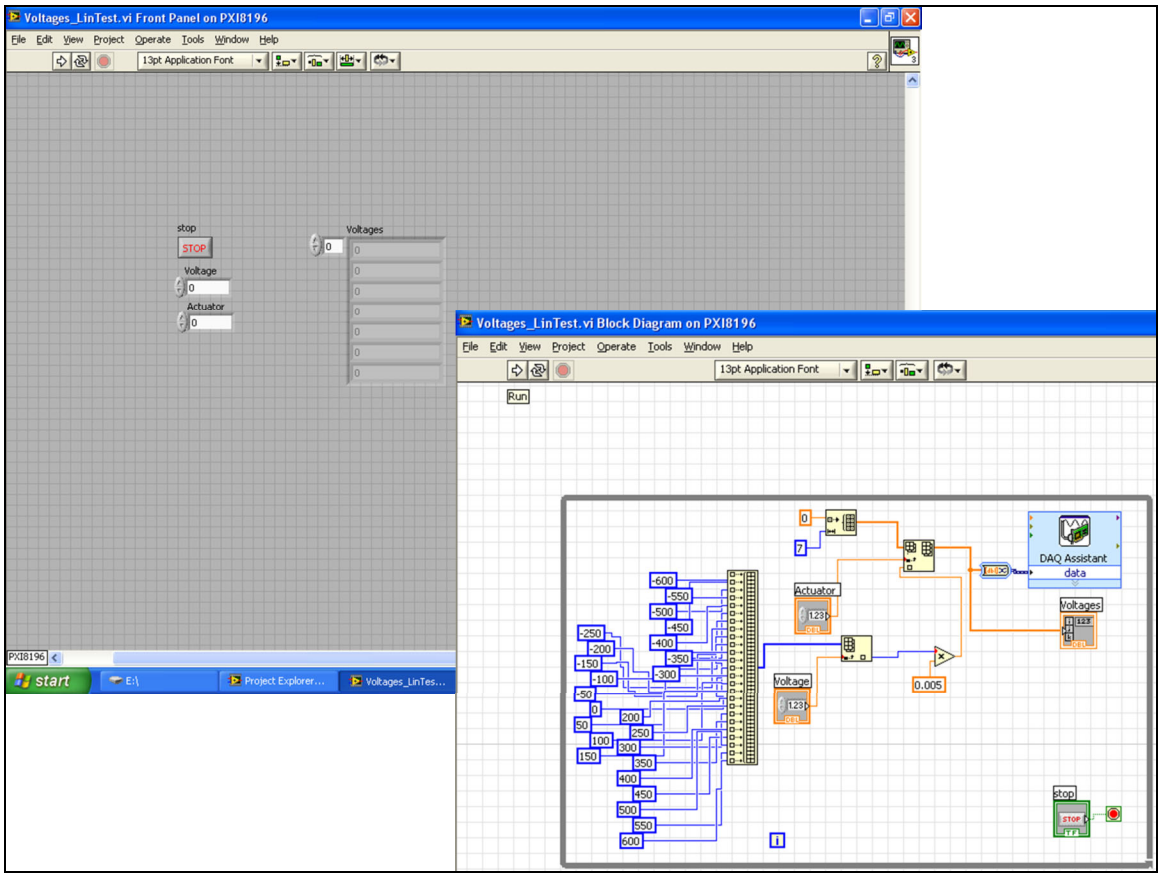

B.4.1 Control VI Block Diagram

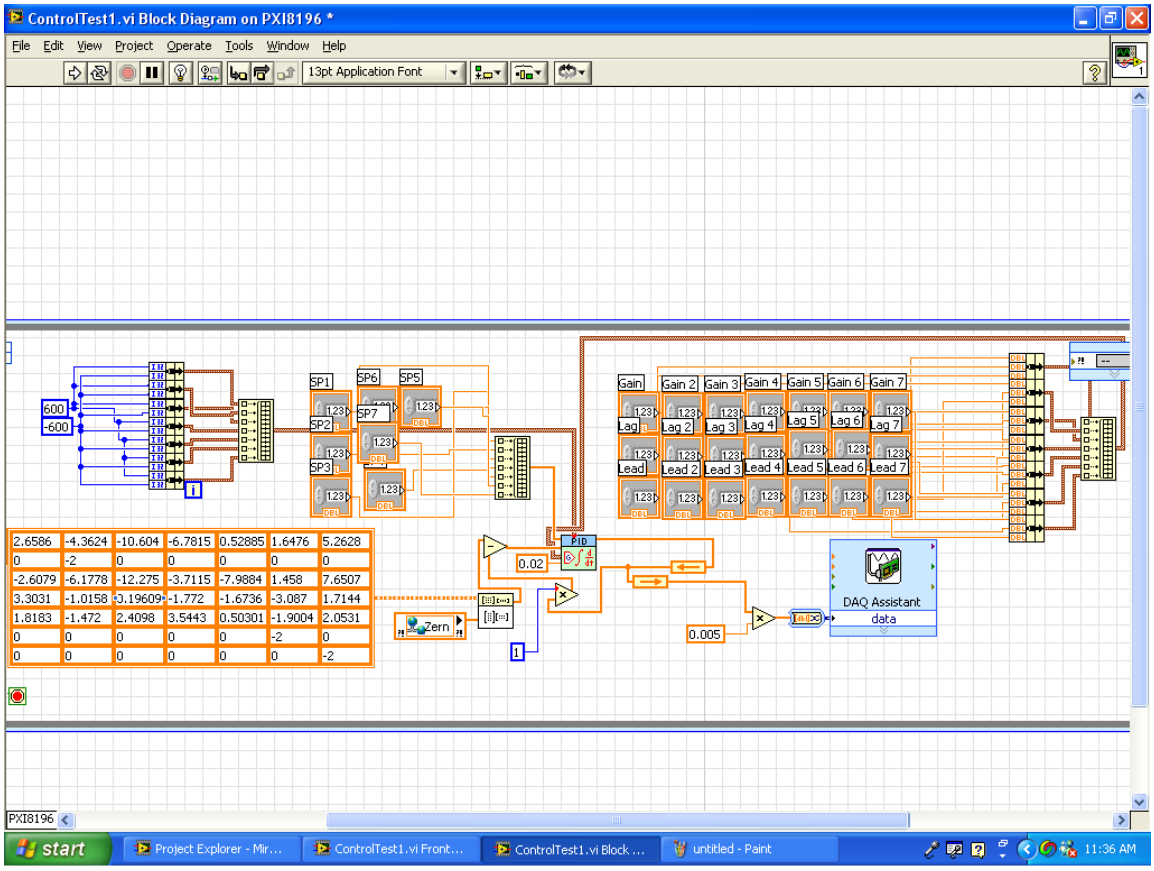

B.4.2 Control VI

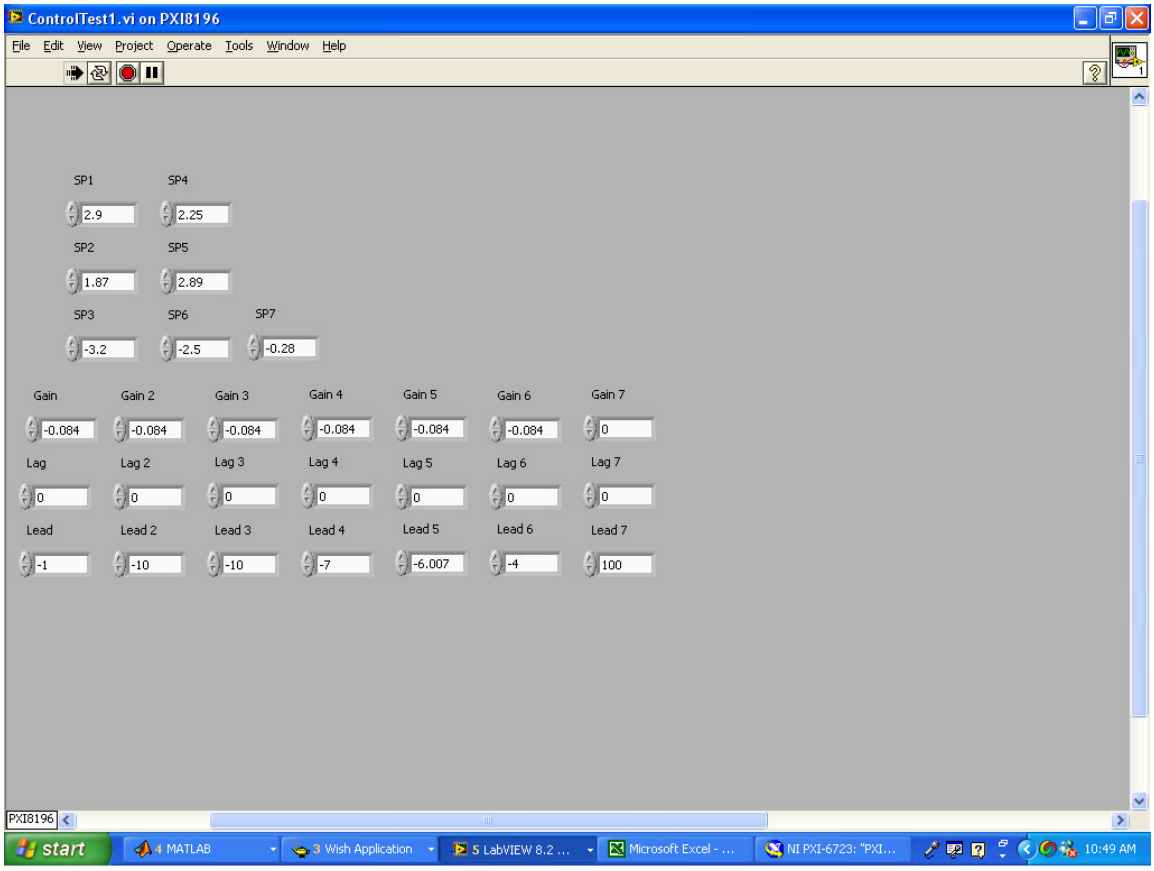

B.5 PiezoStack Control VI

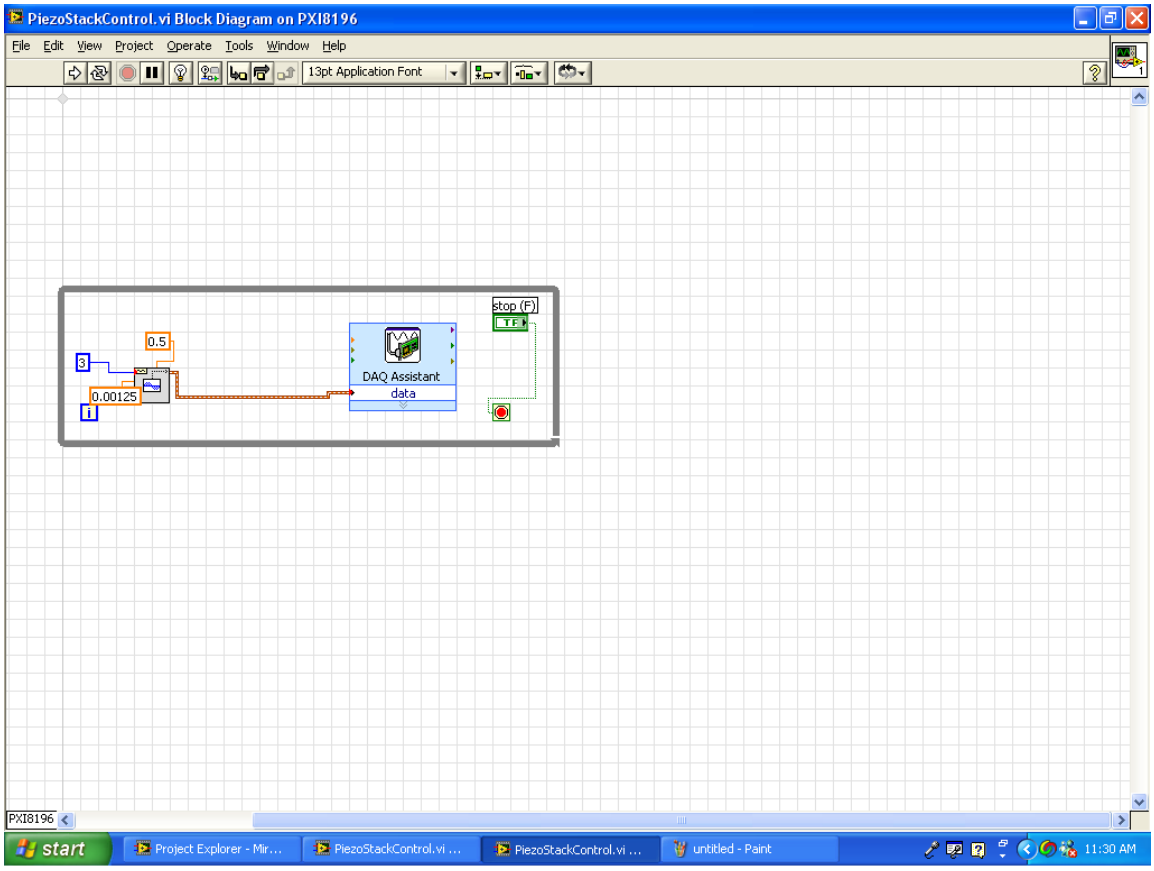

B.6 Zero Volts VI

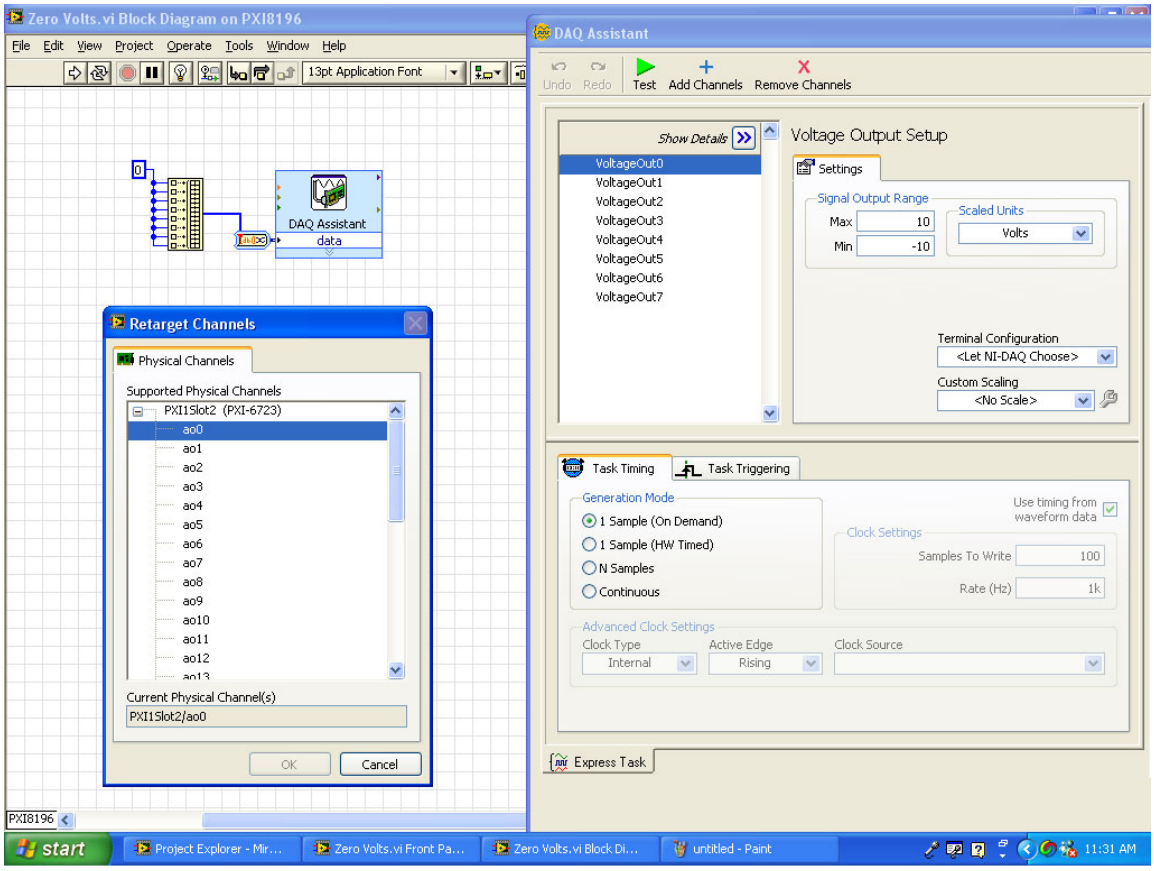

Appendix C. Lab Checklist

1. Turn On Power
    a. Wavescope
    b. Labview PXI Chassis
    c. Laser
2. Capacitance Check
    a. Prior to turning on amplifiers it is crucial to ensure that there is a capacitance on every actuator by checking that the voltage out from the amplifiers using the mirror ground.
    b. The capacitance of 52 micron PVDF is approximately 1.31 nf/in^2 [20]
    c. Turn on all amplifiers
3. Open Wavescope Software.
    a. If alignments haven't changed
        i. On menu bar, select **Camera, Manual, Pupil**
            1. This is done to ensure that the target signal is in the focal plane.
        ii. Next select, **Camera, Camera Settings**
            1. Ensure that the right window, exposure time and frames per second are selected for the test you are planning to run.
        iii. Open the desired test
        iv. Select continuous capture
    b. If you suspect alignments have changed (Example: If mirror has moved)
        i. On menu bar, select **Calibration, Automated**

1. By selecting the automated calibration, the Wavescope software will step you through the calibration process. Wavescope will determine camera exposure times, as well as dictate whether to turn down the intensity of the source. This is the only time that you will need a reference signal.

ii. Next select, **Camera, Camera Settings**

1. Ensure that the frames per second are selected for the test you want to run.

iii. Open the desired test

iv. Select continuous capture

4. Open Labview

a. Open desired project

b. Run test

Appendix D. Mirror Fabrication Notes

1. Sand aluminum ring with appropriate grit sand paper to remove and blemishes or defects from the entire surface.
2. Clean aluminum ring with water or isopropyl alcohol to ensure all dust and dirt is removed from the ring.
3. Roll out enough PVDF to stretch across the mounting structure, and lay it out on a clean flat surface.
    a. Etch the entire surface with Ferric Chloride Acid leaving the bottom side un-etched.

4. Again using water or isopropyl alcohol, clean the residue created from etching the copper off of the PVDF.

5. The opposite side needs to remain un-etched. This will ensure that the PVDF is uniformly grounded to the aluminum ring.
6. Fit the PVDF over the mounting ring ensuring that the etched portion encompasses the entire mounting ring.
7. After placing tensioning ring over PVDF equally space the tensioning clamps around the perimeter of the ring and slowly increase the tension uniformly across the surface of the PVDF until the surface is taunt.
8. Apply epoxy to the face of the aluminum ring paying attention to making the epoxy layer as thin and uniform as possible.
9. Place the aluminum ring epoxy side down on the taunt PVDF keeping the ring a centered as possible within the mounting ring.

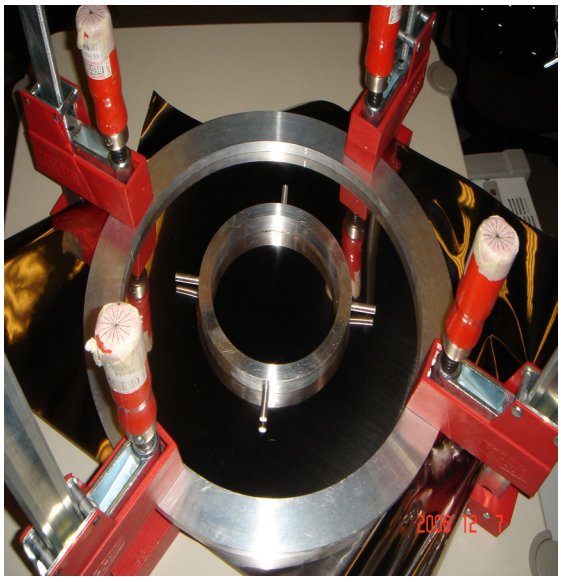

10. Place a one pound plate over the other face of the aluminum ring again making sure that it is centered, this will ensure a uniform bond.

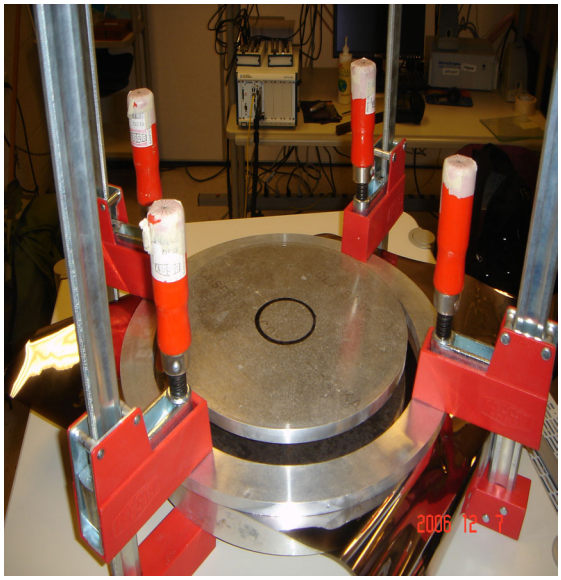

11. Even though a 5-minute epoxy has been applied the curing process will continue for 2-3 days so the setup should not be touched.
12. The next step is carefully remove all of the weight on top of the mirror and then remove the tensioning clamps making certain that the bond between the ring and PVDF is not damaged.

13. Using a razor blade remove the excess PVDF remembering to leave a 1 to 1.5 inch margin around the edge of the aluminum ring to prevent inadvertent grounding.

Appendix E. TCL Scripts for Wavescope

This section highlights the TCL scripts and code necessary to change the Wavescope data format from ASCII to binary.

E.1 Socket.tcl

```
#  fconfigure $newSock -translation {auto crlf}
# To use binary model, comment line above and uncomment two lines below
  fconfigure $newSock -blocking 0
  fconfigure $newSock -encoding binary
  fileevent $newSock readable "SockCommand $newSock"
  set remote_sock $newSock
```

E.2 TestEx.tcl

```
# To use binary model, comment line below and uncomment other lines
               puts $remote_sock [a.dump ws_results(Zernike)]
#              set dmpstr [a.dump ws_results(Zernike)]
#              set ascstr [regsub -all {[(<>\n)]} $dmpstr ""]
#              For Wavescope
#              set binstr [binary format f$wsParam(NZerns) $ascstr]
#              For D-Space
# suggested    set binstr [binary format f84 $ascstr]
#              puts $remote_sock $binstr
```

Bibliography

1. Agnes, G. S. and others, "Shaping of Parabolic Cylindrical Membrane Reflectors for the DART Precision Test Bed," *American Institute of Aeronautics and Astronautics*, 1661:1–12 (2004).
2. Bar-Cohen, Y. "Electroactive Polymers (EAP) As Actuators for Potential Future Planetary Mechanisms". *Evolvable Hardware, 2004. Proceedings. 2004 NASA/-DoD Conference on*, 309-317, 2004.
3. Burge, J. H. and others. "Active Mirror Technology for Large Space Telescopes," *UV, Optical,and IR Space Telescopes and Instruments*, Proceedings of SPIE, 4013:640–648 (2000).
4. Choi, S. H., K. D. Song, W Golembiewskii, S. H. Chu, and G. C. King. "Microwave Power for Smart Material Actuators". *Smart Materials and Structures*, 1:38-48, 2004.
5. Dargaville, T. R., M. C. Celina, P. M. Chapyla, and R. A. Assink. "Evaluation of Piezoelectric PVDF Polymers for Use in Space Environments". *45th AIAA/ASME/ASCE/AHS/ASC Structures, Structural Dynamics, and Materials Conference*, volume 2004-1547. American Institute of Aeronautics and Astronautics, 2004.
6. Das, A., J. M. Sater, C. R. Crowe, and R. Antcliff. *An Assessment of Smart Air and Space Structures: Demonstrations and Technology Descriptive Note: Final rept. Sep 1998-Sep 2000*. Technical report, Institute for Defense Analyses Alexandria VA, 2000.
7. Dimitry, G. and others, . "Distributed Localized Shape Control of Gossamer Space Structures,"American Institute of Aeronautics and Astronautics, 1197:1–8 (2001).
8. Geyl, R., Cayrel, M. "Low CTE Glass, SiC & Beryllium for lightweight mirror substrates." *Optical Fabrication, Testing, and Metrology II*, volume 5965, 2005.
9. Hadinata, P. C. and J. A. Main. "Time Response of Electron Gun Strain Control of Piezoelectric Materials". N. M. Wereley (editor), *Smart Structures and Materials 2000: Smart Structures and Integrated Systems*, volume 3985, 378-384. SPIE, 2000.
10. Hadinata, P. C. and J. A. Main. "Survey of Piezoelectric Material Strain Response to Electron Gun Excitation". L. . P. Davis (editor), *Smart Structures and Materials 2001: Smart Structures and Integrated Systems*, volume 4327, 331-341. SPIE, 2001.
11. Hardy, J. W. *Adaptive Optics for Astronomical Telescopes*. Oxford University Press, 1998.
12. Hiddleston, H. R. and others, . "Comparisons of Deformable Mirror Models and Influence Functions," SPIE: Active and Adaptive Optical Systems, 1542:20–33 (1991).
13. Hill, L., G. Carman, D. G. Lee, and B. Patrick. "Shape Memory Alloy Film for Deployment and Control of Membrane Apertures". H. A. MacEwen (editor), *UV/Optical/IR Space Telescopes: Innovative Technologies and Concepts*, volume 5166, 271-280. SPIE, 2004.
14. Huang, C., R. Klein, F. Xia, H. Li, Q. M. Zhang, F. Bauer, and Z. Y. Cheng. "Poly(vinylidene Fluoride-trifluoroethylene) Based High Performance Electroactive Polymers". *Dielectrics and Electrical Insulation, IEEE Transactions on [see also Electrical Insulation, IEEE Transactions on]*, 11(2):299-311, 2004.

15. *Hubble Space Telescope Specifications*. Retrieved 20 Jan 2007, from https://hubble.nasa.gov/index.php
16. *JWST Update.* Retrieved 20 Jan 2007, from http://hubblesite.org/newscenter/archive/releases/miscellaneous/2003/27/text.
17. Kutz, M. *Handbook of Materials Selection*. J. Wiley, 2002.
18. Lutz, B. J. *Axisymmetric Optical Membrane Modeling Based on Experimental Results*. masters, Air Force Inst of Tech, 2004.
19. Madden, J. D., N. A. Vandesteeg, P. A. Anquetil, P. G. Madden, A. Takshi, R. Z. Pytel, S. R. Lafontaine, P. A. Wieringa, and I. W. Hunter. "Artificial Muscle Technology: Physical Principles and Naval Prospects". *Oceanic Engineering, IEEE Journal of*, 29(3):706-728, 2004.
20. Main, J. A., G. C. Nelson, and J. W. Martin. "Electron Gun Control of Smart Materials". M. E. Regelbrugge (editor), *Smart Structures and Materials 1998: Smart Structures and Integrated Systems*, volume 3329, 688-693. SPIE, 1998.
21. Menikoff, A. "Actuator Influence Functions of Active Mirrors," Applied Optics, Vol. 30, No.7:833–838 (March 1991).
22. Measurement Specialties, *Piezo Film Sensors Technical Manual*. Measurement Specialties, Inc. 1999.
23. Nelson, G. C., J. A. Main, and J. W. Martin. "Wavefront Conjugation Using Electron-Gun-Controlled Piezoelectric Materials". P. L. Wizinowich (editor), *Adaptive Optical Systems Technology*, volume 4007, 582-589. SPIE, 2000.
24. Paquette, J. W. and K. J. Kim. "Ionomeric Electroactive Polymer Artificial Muscle for Naval Applications". *Oceanic Engineering, IEEE Journal of*, 29(3):729-737, 2004.
25. Patrick, B., J. Moore, S. Chodimella, D. Marker, and B. deBlonk. "Final Testing and Evaluation of a Meter-Class Actively Controlled Membrane Mirror". *47th AIAA/ASME/ASCE/AHS/ASC Structures, Structural Dynamics and Materials Conference*, volume AIAA-2006-1901. American Institute of Aeronautics and Astronautics, Inc., 2006.
26. Peterson. *Control Demonstration of a Thin Deformable In-Plane ActuatedMirror*. masters, Air Force Inst of Tech, 2006.
27. Pollard, E. L. and C. H. Jenkins. "Shape Memory Alloy Deployment of Membrane Mirrors for Spaceborne Telescopes". *47th AIAA/ASME/ASCE/AHS/ASC Structures, Structural Dynamics and Materials Conference*, volume AIAA-2005-2196. 2005.
28. Schmidt, V., et al. "Manufacturing of light-weight laser mirror substrates with low thermal expansion." *Laser Resonators and Beam Control VIII,* volume 5708, SPIE, 2005.
29. Sessler, G. M. and A. Berraissoul. "Tensile and Bending Piezoelectricity of Single-film Pvdf Monomorphs and Bimorphs". *Electrical Insulation, IEEE Transactions on [see also Dielectrics and Electrical Insulation, IEEE Transactions on]*, 24(2):249-254, 1989.
30. Shepherd, M. J. *Lightweight ynamic In-Plane Actuated Deformable Mirrors for Space Telescopes.* PhD, Air Force Inst of Tech, 2006.
31. Shih, H. R., R. Smith, and H. S. Tzou. "Photonic Control of Cylindrical Shells with Electro-Optic Photostrictive Actuators". *AIAA Journal*, 42(2):341-347, 2004.

32. Shih, H. R. and H. S. Tzou. “Opto-Electromechanical Actuator Patches For Active Vibration Control Of Thin Plates". *42nd AIAA/ASME/ASCE/AHS/ASC Structures, Structural Dynamics, and Materials Conference*, volume AIAA-2001-1556. 2001.
33. Sobers, D. M. *Smart Structures for Control of Optical Surfaces*. masters, Air Force Inst of Tech, 2002.
34. Sobers, D. M., G. S. Agnes, and D. Mollenhauer. “Smart Structures for Control of Optical Surfaces". *44th AIAA/ASME/ASCE/AHS/ASC Structures, Structural Dynamics, and Materials Conference*. American Institute of Aeronautics and Astronautics, Inc., 2003.
35. Steel, M. R., F. Harrison, and P. G. Harper. “The Piezoelectric Bimorph: an Experimental and Theoretical Study of Its Quasistatic Response". *J. Phys. D: Appl. Phys.*, 11(6):979-989, 1978.
36. Steinhaus, E. and S. G. Lipson. “Bimorph Piezoelectric Flexible Mirror". *Journal Optical Society of America*, 69(3):478-481, 1979.
37. Sumali, H., J. E. Massad, P. L. Reu, P. L. Chaplya, and J. W. Martin. “Analytical and Experimental Studies of Orthotropic Corner-Supported Plates with Segmented In-Plane Actuators". *2005 ASME International Mechanical Engineering Congress and Exposition*. American Society Of Mechanical Engineers, 2005.
38. *The Military Use of Space: A Diagnostic Assessment*, Barry D. Watts, Retrieved on 20 Jan 2007, from www.csbaonline.org
39. Thorburn, W. G. and Kaplan, L. “A Low Voltage Electrodistortive Mirror System for wavefront Control,” SPIE, 1543:52–64 (1991).
40. Trad, E. M. *Dynamic Characterization of Thin Deformable PVDF Mirror*. masters, Air Force Inst of Tech, 2005.
41. Tung, S., S. R. i. ., L.A. Roe, A. Silano, .. P. Maynard, and F. . “A MEMS-based Flexible Sensor and Actuator System for Space Inflatable Structures". *Smart Materials and Structures*, 6:1230-1239, 2001.
42. Wagner, J. W. *Optical Meterology of Adaptive Membrane Mirrors*. masters, Air Force Inst of Tech, 2000.
43. Wagner, J. W., G. S. Agnes, and E. Magee. “Optical Metrology of Adaptive Membrane Mirrors". *Journal of Intelligent Material Systems and Structures*, 11:837-847, 2000.
44. Wang, P. K. C. and Hadaegh, F. Y. “Modal Noninteracting Controls for Deformable Mirrors,” Second IEEE Conference on Control Applications, Vancouver, B.C., 121–128 (September 1993).
45. Yang, E. H. and others. “Design and Fabrication of Electrostatic Actuators with Corrugated Membranes for MEMS Deformable Mirror in Space,” *Imaging Technology and Telescopes*, Proceedings of SPIE, 4091:83–89 (2000).

REPORT DOCUMENTATION PAGE

Form Approved
OMB No. 074-0188

1. REPORT DATE *(DD-MM-YYYY)*	2. REPORT TYPE	3. DATES COVERED *(From – To)*
22-03-2007	Master's Thesis	August 2005 – March 2006

4. TITLE AND SUBTITLE
ACTIVE CONTROL OF A THIN DEFORMABLE IN-PLANE ACTUATED MIRROR

5a. CONTRACT NUMBER

5b. GRANT NUMBER

5c. PROGRAM ELEMENT NUMBER

6. AUTHOR(S)
Gabriele, Thomas Paul., Captain, USAF

5d. PROJECT NUMBER

5e. TASK NUMBER

5f. WORK UNIT NUMBER

7. PERFORMING ORGANIZATION NAMES(S) AND ADDRESS(S)
Air Force Institute of Technology
Graduate School of Engineering and Management (AFIT/EN)
2950 Hobson Way, Building 640
WPAFB OH 45433-8865

8. PERFORMING ORGANIZATION REPORT NUMBER
AFIT/GA/ENY/07-M07

9. SPONSORING/MONITORING AGENCY NAME(S) AND ADDRESS(ES)
NA

10. SPONSOR/MONITOR'S ACRONYM(S)
AFRL/VS

11. SPONSOR/MONITOR'S REPORT NUMBER(S)

12. DISTRIBUTION/AVAILABILITY STATEMENT
APPROVED FOR PUBLIC RELEASE; DISTRIBUTION UNLIMITED.

13. SUPPLEMENTARY NOTES

14. ABSTRACT
Previous work done in the area of active control for surface stabilization and shaping of a deformable membrane mirror at the Air Force Institute of Technology has demonstrated that active control with a simple gain correction is possible using a quasi-static closed-loop feedback on an in-plane actuated deformable membrane mirror. This research builds on that work beginning with the implementation of a new data acquisition system to increase the throughput of the current system. Next, recommended fabrication technique changes are implemented to create a new five-inch membrane-like optical mirror. Lastly, using this new equipment setup, this research begins the process of developing a non-linear controller to actively damp out higher frequency disturbances. The overall goal of providing greater system bandwidth and control of multiple Zernike polynomials has been initially demonstrated.

15. SUBJECT TERMS
membrane mirror, deformable, PVDF, actuation

16. SECURITY CLASSIFICATION OF:			17. LIMITATION OF ABSTRACT	18. NUMBER OF PAGES	19a. NAME OF RESPONSIBLE PERSON
a. REPORT	b. ABSTRACT	c. THIS PAGE			Richard G. Cobb
U	U	U	UU	99	19b. TELEPHONE NUMBER *(Include area code)* (937) 785-3636, ext 4559 (Richard.Cobb@afit.edu)

Standard Form 298 (Rev. 8-98)
Prescribed by ANSI Std. Z39-18